J. Chem. Sci. (2023) 135:19
https://doi.org/10.1007/s12039-022-02130-5

REVIEW ARTICLE

SpringChem

Role of molecular modelling in the development of metal-organic framework for gas adsorption applications

RESHMA JOSE[a], GARIMA BANGAR[a], SOURAV PAL[b] and GOPALAN RAJARAMAN[a,*]
[a]Department of Chemistry, Indian Institute of Technology Bombay, Powai, Mumbai 400076, India
[b]Department of Chemistry, Ashoka University, Sonepat, Haryana 131029, India
E-mail: rajaraman@chem.iitb.ac.in; s.pal@iiserkol.ac.in; Sourav.pal@ashoka.edu.in

MS received 31 October 2022; revised 31 October 2022; accepted 28 December 2022

Abstract. More than 47,000 articles have been published in the area of Metal-Organic Framework since its seminal discovery in 1995, exemplifying the intense research carried out in this short span of time. Among other applications, gas adsorption and storage are perceived as central to the MOFs research, and more than 10,000 MOFs structures are reported to date to utilize them for various gas storage/separation applications. Molecular modeling, particularly based on density functional theory, played a key role in (i) understanding the nature of interactions between the gas and the MOFs geometry (ii) establishing various binding pockets and relative binding energies, and (iii) offering design clues to improve the gas uptake capacity of existing MOF architectures. In this review, we have looked at various MOFs that are studied thoroughly using DFT/periodic DFT (pDFT) methods for CO_2, H_2, O_2, and CH_4 gases to provide a birds-eye-view on how various exchange-correlation functionals perform in estimating the binding energy for various gases and how factors such as nature of the (i) metal ion, (ii) linkers, (iii) ligand, (iv) spin state and (v) spin-couplings play a role in this process with selected examples. While there is still room for improvement, the rewards offered by the molecular modelling of MOFs were already substantial that we advocate experimental and theoretical studies to go hand-in-hand to undercut the trial-and-error approach that is often perceived in the selection of MOFs and gas partners in this area.

Keywords. Metal-Organic Frameworks; DFT calculations; molecular modelling; gas storage and adsorption; spin-state; spin-coupling.

1. Introduction

The need for promising and unconventional energy-conversion methodologies that are environmentally friendly and viable is crucial for meeting the dramatically growing energy demand and reducing the dependence on the combustion of non-renewable fossil fuels.[1–7] As the global energy source is majorly dominated by fossil fuels, minor variations can significantly influence efforts to reach sustainability.[8] Fossil fuels are the major source of primary energy consumption. Non-renewable sources such as natural gas, coal, and oil dominate the list and account for around 80% of the primary energy consumption, and the combustion of these fossil fuels releases greenhouse gases such as CO_2 and CH_4 and contributes to 99.5% of greenhouse gas emission (GHC). It is essential to minimize the pervasive usage of fossil fuels; therefore, the transition to non-fossil fuel energy is essential. In this regard, many promising energy-conversion technologies have been proposed, widely explored, and developed in recent years for extensive use of clean energy, including fuel cells, water splitting, and the use of gases as energy carriers for electric power generation and long-term energy storage methods, etc.[9–17] Besides, all these energy conversion strategies that are broadly established to content energy crisis, the possibility of gas as an energy carrier, which can replace carbon-based fuels, offers wide possibility as it is a clean and safe method of storing energy. Though it is a welcoming and effective energy carrier, implementing various gases as an alternative for hydrocarbons and their conversion to energy is challenging due to their low volumetric energy density and flammability. The cryogenic distillation method for storage and separation of gases by compressing the gases at very high pressure is a challenging task considering the huge practical implications. To overcome

*For correspondence

Published online: 14 March 2023

this challenge, we need to design cheap and lightweight materials that can reversibly separate and store gases quickly and efficiently near ambient conditions. Thus, developing a secure and functional gas absorptive and separative system with high surface area, gas uptake, and low density is of great interest in today's scenario.[2]

Various gas storage materials such as zeolites, Covalent Organic Frameworks (COFs), and Metal-Organic Frameworks (MOFs) are reported in the literature. Zeolites are a class of aluminosilicate materials with a highly crystalline nature, comprised of a network of linked cavities and molecular pores with sieving properties.[18,19] Their peculiar properties, such as high thermal stability, large ion-exchange capacity, and caged structure, make them good encapsulating agents for nonpolar gases.[20]As the zeolites are readily available, low cost, robust, and easy to synthesize, they are beneficial over other microporous materials.

These materials' physical and chemical properties can be tuned and offer a variety of chemical compositions due to their ion exchange ability. The gas storage and separation in these microporous materials depend on factors such as the interaction of molecules with the internal surfaces of the micropores, optimal storage temperature, etc. Since the adsorption of molecules into the cavity of zeolites was occurring at high-pressure and low-temperature conditions, the practical use of zeolites for gas storage and separation was a limiting case. Further, the Zeolites have other disadvantages, such as they are hard to regenerate once utilized, it is hard to reuse the adsorbed materials, and they can not be fine-tuned at will for any specific gas applications (O_2 vs N_2, etc.)

Covalent organic frameworks (COFs) comprise mainly organic linkers formed by boron oxide clusters through covalent bonds. They possess low densities than MOFs and have a large surface area and pore volume. COFs also has various applications in gas storage, catalysis, etc. The electrostatic contribution of framework charges in COFs is found to be smaller than that in MOFs. The limiting factor is the strong interaction of gas molecules with the COFs, as the host-guest interactions are often covalent in nature. Also, the covalent organic frameworks are not crystalline, which limits their application in various industrial processes. Besides zeolites and COFs, several hydrogen storage systems, such as conventional hydrides, complex hydrides, sorbent systems, and chemical hydrides are also available in the literature for gas storage and separation applications.

Although zeolites, COFs, and interstitial hydrides have emerged as gas storage/separation systems, they did not have large-scale industrial applications due to their less thermal stability, loss of crystalline nature, etc. Many strategies have come forth to improve the efficiency of gas uptake systems. Among all, MOFs based adsorptive gas storage system is envisioned as a long-term solution for an efficient gas uptake platform and replacement for carbon-based fuels.[21,22] MOFs represent crystalline coordination polymers, which belong to a class of porous polymeric materials with numerous applications.[23–32] They are peculiar absorbent materials constructed from secondary building units of metal-containing nodes and organic linking groups and are also known as porous coordination polymers (PCPs).[33] MOF chemistry is ubiquitous and one of the rapidly expanding research fields in chemistry due to its appealing functional and structural tunability.[34,35] The endlessly arising unique structures, research publications, numerous citations, and consistent enlargement of research ambit elucidate the same. The advancement in cluster chemistry, sophisticated organic synthesis pertaining to post-synthetic modification and ligand design, and progress in structure resolving through X-ray crystallography are attributed to the ever-expanding and extraordinary rise of MOF research. A signature of MOF is their crystallinity. The crystalline nature makes effortless structural characterization *via* X-ray diffraction, along with symmetry-adapted design techniques like the reticulate approach, enabling the prudent architecture of MOF topology.[36] This permits the meticulous discovery of MOFs, unlike the trial-and-error discovery of conventional solid-state materials in a black box approach. Due to their appealing properties such as structural and functional diversity, porous nature, size tunability, and enormous surface area. MOF is an attractive candidate for their potential applications in gas storage,[37–42] molecular separation,[40,43–50] sensors,[51–56] and catalysis[57–64] among all other classical sorbent systems. The balance between the high gravimetric and volumetric adsorptive capacity of MOF makes them undeniably, a promising class of material for adsorptive gas storage application, apart from zeolites, COFs, and complex hydrides that are available for gas adsorption applications.[65,66] The tuning of MOF-based gas adsorptive systems can give rise to the creation of gas-based energy production and help secure the global ecosystem; for e.g., removing large amounts of carbon dioxide, methane, and nitrous oxide is essential for limiting global warming effects. The selective separation/storage of gases such as hydrogen and methane is imperative for the prominent use of clean energy. To obtain a pure form of oxygen, cryogenic separation is the traditional method

followed by industries; however, it requires extensive infrastructure and high-pressure conditions, limiting scalability and portability. As oxygen and nitrogen kinetic diameters are undoubtedly close to 3.46 Å and 3.64 Å, respectively, the membrane-based separation cannot be made practical. In this scenario, sorbent system-based trapping of oxygen is of great promise. Thus, MOFs serve as suitable candidate for the selective separation of gases due to their porous nature, enormous surface area and pore volume.

As geometry and structure play a vital role in gas adsorption in MOFs, several groups engaged in synthesizing and characterizing new MOF materials and tested them for various gas adsorption. The strategy employed includes the introduction of organic donor moieties with enhanced donor capability, increasing the coordination number of the open metal sites, and doping with other metals. While impressive progress had been made in terms of selectivity and binding for various gases with various MOF architectures such as (i) record high H_2 storage at 60 g H_2/L was achieved with Mn-BTT MOF[67] ($[Mn\text{-}(DMF)_6]_3[(Mn_4Cl)_3(BTT)_8(H_2O)_{12}]_2$) (ii) very high selectivity of O_2 over N_2 and other gases was achieved with Fe_2-dobdc MOF (8.16 mmol/g)[68] (iii) very high uptake for CO_2 of 130 mmol g^{-1} with $[Zn(adc)(4,40\text{-bpe})_{0.5}]$ (ADC = 4,4'-azobenzenedicarboxylate, 4,4′-bpe = trans-bis(4-pyridyl)ethylene)) MOF[69] (iv) very high binding affinity and selectivity achieved with a hydrocarbon such as methane[70] with ~200 cm^3(STP)/cm^3, etc. Despite these impressive records, there is no prescribed protocol to obtain selectivity with any given MOFs. Most of the observations arrived after a heavy screening of hundreds of MOFs in a trial-and-error approach and then fine-tuning the selectivity/binding affinity *via* further experiments (desolvation, solvation, additives, etc.). Understanding the host-guest interaction between the MOFs and the gas is crucial if we need to develop further robust MOF materials.

However, these are challenging from the experimental perspective as obtaining structural or geometric information of MOFs upon gas bindings is often cumbersome. Particularly mimicking the best gas uptake conditions, which often involve high pressure throw up further challenges to get insightful information. Moreover, a search Cambridge structural database reveals a report of 1,10,000 MOF structures (updated still 2020), and a quick glance at the collected data reveals that most of the reported MOFs are paramagnetic, as shown in Figure 1. This adds further complexity as obtaining structural information of gas binding in MOFs using spectral methods such as NMR

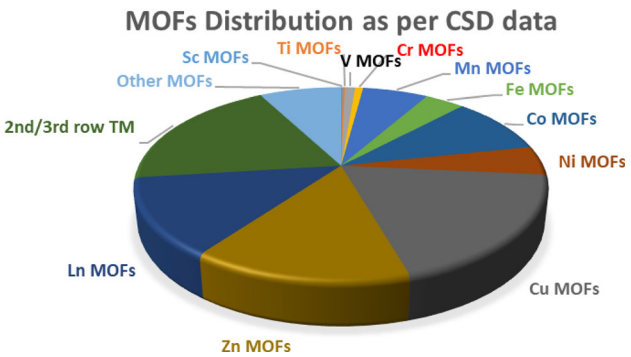

Figure 1. The distribution of MOFs as per CSD database (2020).

is limited for such systems, even though sophisticated methods such as the polarised neutron diffraction method are available. In this regard, computational tools, both classical and quantum mechanical, are invincible, particularly methods based on density functional theory (DFT), which yield structural information upon binding, such as binding site, nature of the binding, uptake capacity at a given site, and binding energy for each of these sites. Combining this information with classical simulation employing Monte-Carlo or forcefield methods could yield further information and the simulation of experimental adsorption isotherm to yield vital design clues for a new generation of MOFs.

Theoretical and computational methods are now widely used for predicting various modifications of MOFs and how the gas adsorption capability of MOFs alters upon varying the coordination environment and metal sites. Among quantum mechanical methods of modeling MOFs, several approaches are followed (i) employ pDFT calculations which mimic the real system and the boundary conditions are enforced (ii) cluster model approach, which aims to focus on small or medium size models corresponding to the repeating units of MOFs for binding (iii) other approaches similar to QM/MM where multiple levels of theory are employed within the same network to reduce the computational cost and at the same time maintain a high level of accuracy and (iv) there are also other approaches such as quantum Monte-Carlo which take inputs from DFT calculations to generate insights.

In this review article, we aim to focus on various theoretical studies based on DFT calculations performed to understand the nature of binding of gases such as CO_2, H_2, O_2, and CH_4 on various MOF containing first-row transition elements with some selected examples to have birds-eye-view on the role of metal ions and ligand linkers in obtaining selectivity and uptake capacity.

2. Modelling carbon-dioxide capture in MOFs

CO_2 is an abundant gas in the earth's atmosphere, and due to the industrial revolution and increased fossil fuel usage, CO_2 emission has been much higher in the last decade. The rising level of CO_2 in the atmosphere is the primary cause of the greenhouse gas effect, global warming, and climate change. Due to this increasing environmental threat, several kinds of research have been conducted for the effective capture of CO_2 and conversion to useful gases. Among the various strategies available for capturing CO_2, material-based storage is a more effective and less energy-consuming technique for regeneration.

There are several efforts to capture CO_2 in MOFs, which can be further utilized for CO_2 sequestration. As modeling CO_2 in MOFs requires extensive benchmarking of exchange-correlation functionals and the role of dispersive interaction in the estimation of binding energy, the work of Siegel and co-workers[71] assumes importance. In this work, the authors have compared the BE with respect to the experimental enthalpies (ΔH) of CO_2 adsorption on four variants of M_2(dobdc) (M = Mg-DOBDC,[72] Ni-DOBDC,[72] and Co-DOBDC[73]) (Figure 2a) and Cu-HKUST-1[74] based on a series of GGA[75] functionals (optB86b, optB88, optPBE, revPBE, and rPW86) using VASP suite[76] employing projector-augmented-wave (PAW) method[77] including Grimme's dispersion correction (DFT-D2).[75,78–80] The studies show that the revPBE-vdW functional predicts the BE well; however, the metal-oxygen (CO_2) distances were overestimated. Despite largely capturing the BE trends, the LDA and GGA functionals considerably overbind (LDA) and underbind (GGA) CO_2 in comparison to experimental enthalpies. When employing "off the shelf" DFT-D2 parameters to add a semiempirical r^{-6} dispersion term to the GGA exchange-correlation energy, the trends and amplitude of the adsorption enthalpies are much improved. However, on average, this method under binds CO_2 by 7 kJ/mol (18%) in comparison to the experimental observation. Some of the nonempirical vdW density functionals provide better accuracy, with the revPBE-based functional[81] having an average inaccuracy of only 2 kJ/mol (4%) in comparison to the experiment.[81] The revPBE functional overestimates the length of the metal–CO_2 bond by roughly 10%; thus, this gain in energetics is followed by a minor decline in the accuracy of predicted structures.[82] For materials intended for carbon capture applications, long-range van der Waals interactions are essential for estimating thermodynamic features. The efficiency and reliability of revPBE-vdW functional indicate the potential of density functional methods for quick screening of possible CO_2 adsorbents (Figure 3). These approaches have advantages over costly, cluster-based quantum-chemical approaches as they can handle the large, periodic unit cells that are typical of MOFs. While the DFT-D2 was state-of-the-art back then, a better and improved version of dispersion corrections has been reported,[75,78,79] whose role in geometry and structures are not yet established. Further, it is common knowledge that incorporation of HF exchange improves both the structure and energies, but extensive benchmarking involving hybrid, double-hybrid functionals are still lacking.

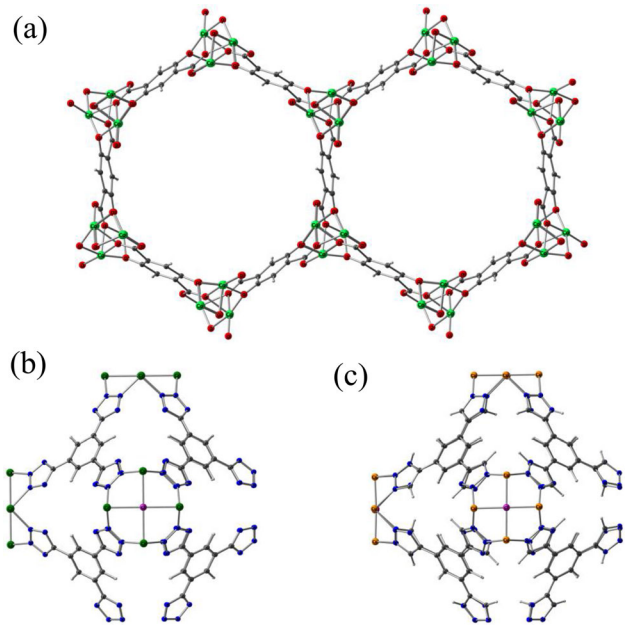

Figure 2. The representative structures of MOF chosen for the investigation of modelling of CO_2 adsorption in MOFs. (a) Co-DOBDC, (b)Cr-BTT, and (c) Cu-BTTri. Co, Cr, Cu, O, N, Cl, C, and H are denoted as light green, dark green, orange, red, blue, purple, gray, and white, respectively.

As dispersion effects seem to play a critical role, *ab initio* approaches such as MP2[83] or CCSD(T)[84] methods are expected to be superior, as demonstrated by the work of Snurr and co-workers[85] studies on seven variants of M_2(dobdc) (M= Mg (Mg-dobdc), Mn (Mn-dobdc), Fe (Fe-dobdc), Co (Co-dobdc), Ni (Ni-dobdc), Cu (Cu-dobdc), and Zn (Zn-dobdc); (Figure 2a) to understand the trend in CO_2 uptake. To begin with, authors have performed cluster model, pDFT, as well as QM/MM approach employing MP2 method as QM workhorse. The generalised gradient approximation (GGA) functional PW91 was used for periodic calculations were lattice constants were optimised using local density approximation (LDA) with a kinetic energy cut-off of 520 eV and force on

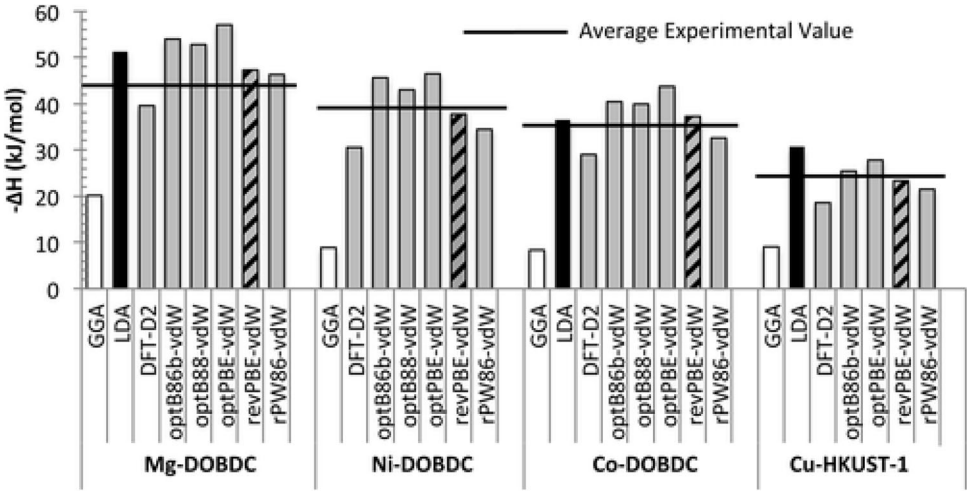

Figure 3. CO_2 adsorption energies in M/DOBDC (M = Mg, Ni, Co) and HKUST-1 calculated using standard density functional methods. Reproduced with permission from Ref. 71. Copyright 2012 American Chemical Society.

each atom less than 0.01eV. The cluster model calculations were performed using the G09[86] suite with hybrid B3LYP[87] functional employing 6-31+G(d) basis set with the energies corrected for the basis set superposition error employing counter-poise correction. The comparison of the experimental isosteric heat of adsorption (42kJ/mol) with employed DFT methods for seven metal series is shown in Table 1. Among the metal studied, Mn, Fe, Co, Ni, and Cu were found to have antiferromagnetic interaction between the metal, leading to an S = 0 diamagnetic ground state, which is attributed to the nature of super-exchange which is mediated here *via* μO(R) group and a carbonate ion (Figure 4). As the ligand field environment presented here is relatively weak, all the metals found to have a high-spin state as their ground state, and this is found to be consistent with the experimental report. The experimental observations that Mg > Ni > Co > Fe > Mn > Zn with the decreasing order of isosteric value for the CO_2 adsorption found to correlate to the charge on the metal ion with larger charges tend to yield lower binding affinity (Table 1). While revPBE-vdW[81] was found to yield better geometries for M_2(dobdc) MOFs, this function has not been tested in this work, though a direct correlation was made to MP2 methods.

Further, to understand the role of open metal sites in controlling the high adsorption enthalpies of CO_2 adsorption and the role of ligand part in adsorption, Long and co-workers investigated a series of M-BTT (Cr-BTT, Mn-BTT, Fe-BTT, Cu-BTT) frameworks (Figure 2b) for CO_2 adsorption.[103] The organic linker part in this framework is the BTT^{3-} ligand (BTT^{3-}=1,3,5-benzenetristetrazolate). As suggested in the work of Siegel and co-workers,[71] the dispersion corrected functional (rev-vdW-DF2 +U) was employed using VASP[89] software to model the non-covalent interactions between CO_2 and framework. The authors have performed pDFT calculations using a plane-wave basis set with a kinetic energy cut-off of 800 eV. The DFT-based structural investigations have suggested that the open metal sites contribute to the

Table 1. The comparison of CO_2 binding energies (in kJ/mol) was calculated using DFT, MP2, and MP2- based QM/MM methods and experimental heats of adsorption Q_{st} (in kJ/mol). Reproduced with permission from Ref. 85 Copyright 2013 from Royal Society of Chemistry.

MOF	LDA periodic	GGA periodic	LSDA cluster	B3LYP cluster	MP2 cluster	QM/MM periodic	Q_{st}
Mg-dobdc	-54.3	-23.9	-63.0	-23.9	-40.5	-48.2	-
Mn-dobdc	-38.4	-13.3	-43.2	-12.1	-30.3	-37.2	42.0
Fe-dobdc	-38.1	-9.4	-36.6	-4.5	-24.2	-32.2	31.9
Co-dobdc	-42.5	-10.6	-43.2	-7.70	-29.7	-37.0	34.3
Ni-dobdc	-43.1	-12.5	-52.9	-11.2	-31.2	-39.1	34.5
Cu-dobdc	-31.0	-6.0	-27.4	-3.5	-16.2	-23.9	38.7
Zn-dobdc	-40.2	-12.4	-50.4	-11.8	-29.7	-37.0	24.0

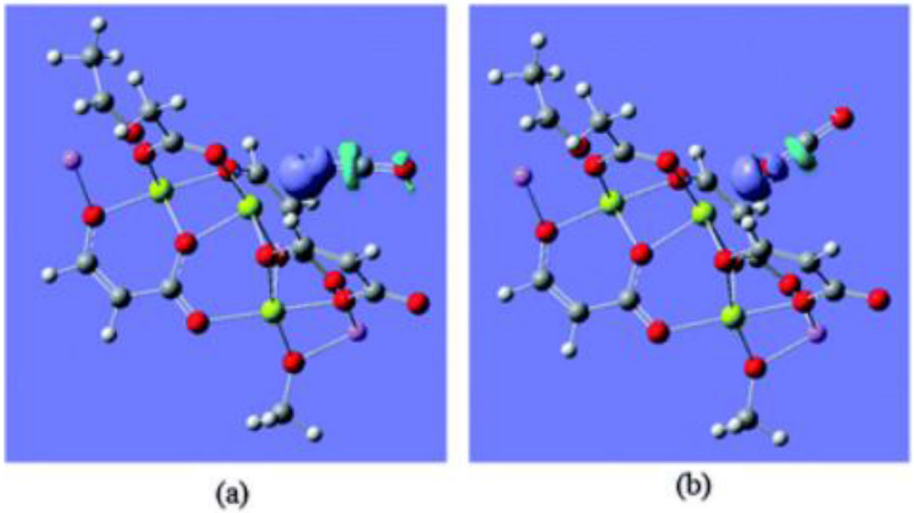

Figure 4. CO_2 charge gain and loss as it is adsorbed to the CPO-27-Mg cluster in a linear configuration. The blue and cyan surfaces represent charge gain and loss, respectively, at an isosurface value of 0.003. White, gray, red, yellow, purple spheres represent H, C, O, Mg, Li atoms, respectively. (a) M–O–C angle is 145.9°; (b) M–O–C angle is 180°. Reproduced with permission from Ref. 85. Copyright 2013 from Royal Society of Chemistry.

maximum absorption of CO_2 in the framework. The predicted linear geometry in the intramolecular CO_2 angles matches the experiments. Notably, the binding energy estimated for the open metal center (site I) is in excellent agreement with the experimentally measured zero-coverage isosteric temperatures of adsorption (Table 2). The computed bond distance for the interaction of CO_2 with metal M–O (CO_2) in site I nearly matches experimental findings with a difference of $\sim$ 0.04 Å in the case of Cr-BTT and Cu-BTT. If we compare the DFT computed binding energies for the metal centre (site I) and nitrogen (site II), the binding strength of CO_2 at site II appears to be not dependent on the metal, the binding energy of CO_2 at the site I depend heavily on the nature of the metal. Sites III and IV have very weak binding compared to sites I and II. In fact, the examined frameworks show just a difference of 2 kJ/mol in the computed binding energy for CO_2 at site II. Even at increased loading of CO_2, the DFT computed results were similar to the experimental uptake capacities. The binding strength at site I is greater than at site II for Fe-BTT, Cr-BTT, and Cu-BTT, which can be attributed to the charge on the metal centre. The trend in adsorption energy follows Fe $>$ Cr $>$ Cu. The overall conclusion of the study is that DFT investigations are a useful tool to unveil the importance of the open metal site in the M-BTT and the unique role of the nature and charge on the metal centers in enhancing the CO_2 uptake capacity.

Further in the line of employing the BTT family of ligands for gas adsorption, Queen and co-workers have investigated Cu-MOFs to understand the peculiar role of ligand functionalization in tuning CO_2 adsorption and N_2 adsorption.[88] The Cu–BTTri ($BTTri^{-3}$ = 1,3,5-benzenetristriazolate) and Cu–BTT (BTT^{-3} = 1,3,5-benzenetristetrazolate) MOFs (Figure 2c) were chosen for the DFT investigations. The electronic structure simulations were performed in Quantum Espresso[90] software using PBE[91] functional, considering the Grimme-D2 dispersion corrections. The spin-polarised calculations suggested an antiferromagnetic ground state for the Cu-BTTri system. The DFT investigation suggested four binding sites for CO_2, with the open metal site, site-I has an estimated binding energy of -21 kJ/mol. The energy decomposition analysis indicated that the major contribution of binding energy is due to the van der Waal interactions (-17.6 kJ/mol). The second site is located above the metal cluster (see Figure 5), and the binding energy for this site is computed to be -26 kJ/mol, which is slightly stronger than site I. The isosurface plot clearly shows the interaction between the electron-rich triazolate group of BTTri ligand and CO_2, rationalizing a significant contribution to the binding energy arising from van der Waal interactions. The electrostatic interaction between negatively charged BTTri ligand and oxygen of the CO_2 leads to a favourable binding at site II. The differences in their electron donor ability due to tetrazolate and triazolate ligand moieties in Cu-BTT and Cu-BTTri is playing a role in controlling the adsorption pattern. The third adsorption site is near the benzene ring, and the binding energy estimated is lower than the site I and II (-17 kJ/mol), as the interaction of CO_2 with weak π-acceptor capability interacts feebly with the π-electron cloud of the benzene ring reducing the overall binding energy for this

Table 2. The comparison of the various MOFs, bound gas studied here, and experimental and theoretical binding energies.

MOF name	Gas	Computational method employed		Computed ΔH_b (kJ/mol)	Qst/BE (kJ/mol)	Ref.
Mg-dobdc	CO_2	revPBE-vdW		-47.3	−44.2 ± 4.6	72, 85, 129–131
		MP2		-40.5		
Ni-dobdc	CO_2	revPBE-vdW		−37.8	−39.6 ± 1.5	72, 129
		MP2		-31.2		
Co-dobdc	CO_2	revPBE-vdW		−37.2	−35.7 ± 1.9	72, 129
		MP2		-29.7		
Cu-HKUST-1	CO_2	revPBE-vdW		−27.7	−23.7 ± 8.2	132–134
Mn-dobdc	CO_2	MP2		-30.3	31.9	85
Fe-dobdc	CO_2	MP2		-24.2	34.3	85
Cu-dobdc	CO_2	MP2		-16.2	24.0	85, 135
Zn-dobdc	CO_2	MP2		-29.7	30.6	85
Cr-BTT	CO_2	rev-vdW-DF2 + U	Site 1	-36.6	36.7	
			Site 2	-26.6		
Mn-BTT	CO_2	rev-vdW-DF2 + U	Site 1	-	45.6	136
			Site 2	-		
Fe-BTT	CO_2	rev-vdW-DF2 + U	Site 1	-51.7	51.2	136
			Site 2	-24.5		
Cu-BTT	CO_2	rev-vdW-DF2 + U	Site 1	-29.4	30.7	136
			Site 2	-26.8		
Cu-BTTri	CO_2	PBE-D2	Site 1	−25.0	22.0	137
			Site 2	−26.5		
			Site 3	−17.0		
			Site 4	−15.8		
Mn-BTT *	H_2	ωB97X-D	Site 1	-17.2	-11.9	103
			Site 2	-7.5	-	
			Site 1+Site 2	-13.6	-10.6	
Cu-BTT*	H_2	ωB97X-D	Site 1	-10.8	-10.4	103
			Site 2	-7.0		
			Site 1+Site 2	-10.1	-9.8	
Zn-BTT*	H_2	ωB97X-D	Site 1	-16.3	-	103
			Site 2	-7.7	-	
			Site 1+Site 2	-14.1	-	
Cu-BTTri	H_2	PBE-D2	Site 1	-10.0	10.5	110
			Site 2	-3.0		
			Site 3	-4.9		
			Site 4	-3.0		
$Sc_3(btc)_2$	O_2	PBE-D2	side-on	-328.0	-	111
$Ti_3(btc)_2$	O_2	PBE-D2	side-on	-329.0	-	111
$V_3(btc)_2$	O_2	PBE-D2	side-on	-158.0	-	111
$Cr_3(btc)_2$	O_2	PBE-D2	bent	-100.0	-	111
$Mn_3(btc)_2$	O_2	PBE-D2	bent	-264.0	-	111
$Fe_3(btc)_2$	O_2	PBE-D2	bent	-45.0	-	111
$Co_3(btc)_2$	O_2	PBE-D2	bent	-81.0	-	111
$Ni_3(btc)_2$	O_2	PBE-D2	bent	-53.0	-	111
$Cu_3(btc)_2$	O_2	PBE-D2	bent	-103.0	-	111
$Zn_3(btc)_2$	O_2	PBE-D2	bent	-22.0	-	111
$Mo_3(btc)_2$	O_2	PBE-D2	bent	-18.0	-	111
$Ru_3(btc)_2$	O_2	PBE-D2	side-on	-105.0	-	111
$Mg_3(btc)_2$	O_2	PBE-D2	bent	-218.0	-	111
$Sc_2(dobdc)$	O_2	PBE-D2	side-on	-215.0	-	111
$Ti_2(dobdc)$	O_2	PBE-D2	side-on	-354.0	-	111
$V_2(dobdc)$	O_2	PBE-D2	side-on	-264.0	-	111
$Cr_2(dobdc)$	O_2	PBE-D2	side-on	-147.0	-	111
$Mn_2(dobdc)$	O_2	PBE-D2	side-on	-116.0	-	111
$Fe_2(dobdc)$	O_2	PBE-D2	side-on	-88.0	-	111
$Co_2(dobdc)$	O_2	PBE-D2	bent	-83.0	-	111
$Ni_2(dobdc)$	O_2	PBE-D2	bent	-79.0	-	111

Table 2. (contd.)

MOF name	Gas	Computational method employed		Computed ΔH_b (kJ/mol)	Qst/BE (kJ/mol)	Ref.
Cu_2(dobdc)	O_2	PBE-D2	bent	-31.0	-	111
Zn_2(dobdc)	O_2	PBE-D2	bent	-21.0	-	111
Mo_2(dobdc)	O_2	PBE-D2	side-on	-267.0	-	111
Ru_2(dobdc)	O_2	PBE-D2	bent	-157.0	-	111
Mg(dobdc)	O_2	PBE-D2	bent	-37.0	-	111
Co-BTTri	O_2	M06/def2-TZVP		-32.8	−34.0	50
Co-BDTrip	O_2	M06/def2-TZVP		−32.0	−47.0	50
Co-BTT	O_2	M06/def2-TZVP		-28.6	-	50
Co-BTP	O_2	M06/def2-TZVP		-47.5	-	50
Co_2Cl_2(BBTA)	O_2	PBE-D3(BJ)+U/PAW		-19.0	-	118
$Co_2(OH)_2$(BBTA)	O_2	PBE-D3(BJ)+U/PAW		-45.0	-	118
Cr-BTT	O_2	PBE-D2		-74.5	-61.0	50, 119
Mg_2(dhtp)	CH_4	LDA		33.0	18.5	70, 82
Mn_2(dhtp)	CH_4	LDA		29.8	19.1	70, 82
Co_2(dhtp)	CH_4	LDA		29.7	19.6	70, 82
Ni_2(dhtp)	CH_4	LDA		34.8	20.2	70, 82
Zn_2(dhtp)	CH_4	LDA		29.7	18.3	70, 82
PCN-14	CH_4	LDA	Site 1[a]	25.0	30.0	
			Site 2[b]	32.0		
			Site 3[c]	5.8		
			Site 4[d]	18.9		
			Site 5[e]	16.5		
PCN-11	CH_4	LDA	Site 1[a]	24.7	14.6	
			Site 2[b]	25.0		
			Site 3[c]	22.0		
			Site 4[d]	19.5		
			Site 5[e]	15.7		
MOF-5	CH_4	LDA		20.7	12.2	70
HKUST-1	CH_4	LDA	Site 1[a]	25.5	18.2	125, 139
			Site 2[b]	24.8		
			Site 3[c]	24.7		
			Site 4[d]	25.0		
			Site 5[e]	22.0		

[a)] open Cu site, [b)] small cage bottom site, [c)] small cage window site, [d)] large cage corner site I, and [e)] large cage corner II, *Calculations were performed on cluster model.

site III. Site IV is the cavity of the Cu-BTTri framework, where the computed binding energy is -15.8 kJ/mol. The adsorbed molecules in site IV interacted with nitrogens of the BTTri ligand at a distance of ~3.2 Å. After investigating the possible binding sites in Cu-BTTri, the author has also compared the binding of CO_2 in the Cu-BTT framework. The substitution of the triazolate with tetrazolate gave rise to a lower overall uptake capacity in Cu-BTTri compared to Cu-BTT, whereas the selectivity obtained over CO_2/N_2 was better for triazolate moiety. This can be attributed to the weak interaction of Cu and CO_2 in the triazolate due to the elongated Cu-C distance. The shorter metal-ligand distances lead to elongated bonds in the z-axis and, thereby, weak interaction with the incoming CO_2 molecule in the case of the tetrazolate counterpart. Hence, the study implies that various factors, such as uptake capacity and selectivity, together control the efficiency of the adsorption, and care must be taken in analyzing each factor controlling the adsorption and separation. This study shows how to modulate the linker groups in MOFs to improve the binding properties of gases and facilitate efficient gas separation.

3. Modelling hydrogen capture in MOFs

Due to the high gravimetric and volumetric capacity, hydrogen can serve as a promising source of clean energy for replacing fossil fuels and implementing fuel cell economy. However, the lack of cost-effective H_2 storage systems remains a challenge as the current method available for large-scale hydrogen storage is the cryogenic method at the cost of energy and

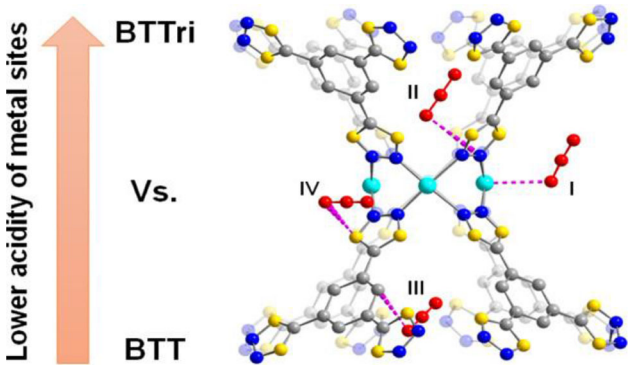

Figure 5. Various binding pockets identified for CO_2 adsorption for Cu-BTT and Cu-BTTri MOF by the DFT calculations. Reproduced with permission from Ref. 88. Copyright 2020 American Chemical Society. The Cu, C, N, are denoted as cyan, gray, and blue spheres, respectively. Yellow spheres represent mixed sites containing both C and N.

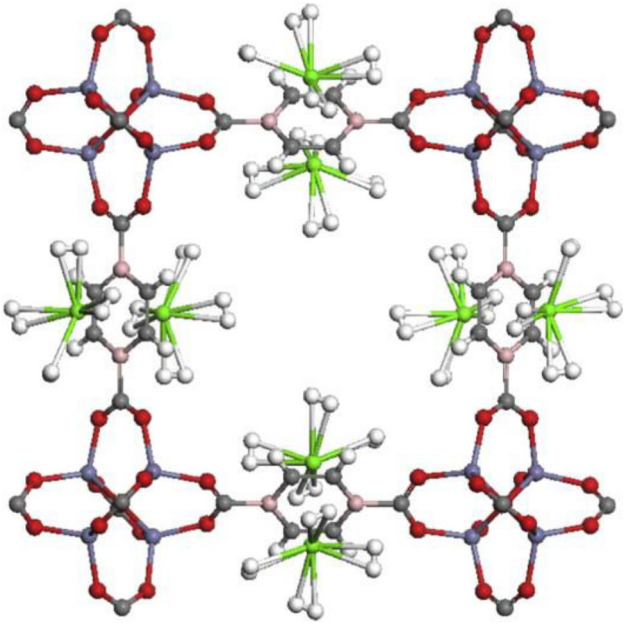

Figure 6. Relaxed structure of Ca-decorated B-substituted MOF-5 with $8H_2$'s adsorbed per linker. The gray, pink, white, red, green and dark violet balls represent carbon, boron, hydrogen, oxygen, calcium and zinc atoms, respectively. Reproduced with permission from Ref.104. Copyright 2009 Elsevier.

infrastructure. Metal-organic frameworks can serve as an appealing hydrogen storage device due to their exceptional diversity and tunability in chemical composition, topological structure, surface chemistry, and large surface area. Understanding the hydrogen adsorption in MOFs through modelling studies offers great interest in this context. Several DFT, coupled-cluster, and symmetry-adapted perturbation theory-based studies[92,93] are available in the literature on various issues related to H_2 binding and uptakes and exploring the possible binding pockets for hydrogen in MOFs.[94–103]

Ihm and co-workers have performed the first principle electronic structure calculations on calcium-decorated and boron-substituted MOF-5.[104] The carbon atoms in the benzene ring of the BDC linker were replaced with two boron atoms at the ortho and para positions. The spin-polarised pDFT calculations were performed in VASP software with the PW91 GGA functional. Figure 6 depicts the BDC (benzene dicarboxylate) linker adorned with calcium atoms and bound hydrogen. The binding energy was estimated before and after boron substitution. The calculations have suggested that the strength of binding between calcium and BDC linker as well as hydrogen molecules and calcium, was improved due to boron substitution. A total of 8 H_2 molecules were binding near the calcium atom with an average binding energy of 20 kJ/mol, which is reasonable for improved hydrogen uptake.

The partial density of the state plot also suggests a favourable interaction between calcium and hydrogen. The peaks corresponding to calcium and hydrogen were found to overlap near the Fermi region. The Kubas interaction of electron donation and back donation between calcium and hydrogen orbitals was evidenced from the partial electron density distribution plot.

In the case of Li and Sc decoration on the BDC linker, the binding energy for hydrogen was ~5 kJ/mol and 31 kJ/mol, respectively, and the elongation of the hydrogen bond distance was comparatively more for the calcium case. Hence the study unveils that the decoration of boron atoms improves the stabilization of calcium on the BDC surface as well as the binding properties of hydrogen in the MOF-5 system.[104]

Pal and co-workers[105] employed *ab initio*, and pDFT-based calculations to explore the impact of light metal (M=Li, Be, Mg, and Al) decoration[104] on the stability and hydrogen adsorption of metal-organic framework MOF-5.[106,107] The DFT calculations were performed by considering a model system where the BDC (benzene dicarboxylate) linker moiety/MOF-5 is stacked with light metal, and the H_2 adsorption is on top of the light metal (Figure 7). The authors aim to understand the stabilizing charge transfer and variation in interaction energy associated with hydrogen adsorption through the light metal decoration.

The idea of metal decoration on the surface is to generate charges on the benzene surface so that

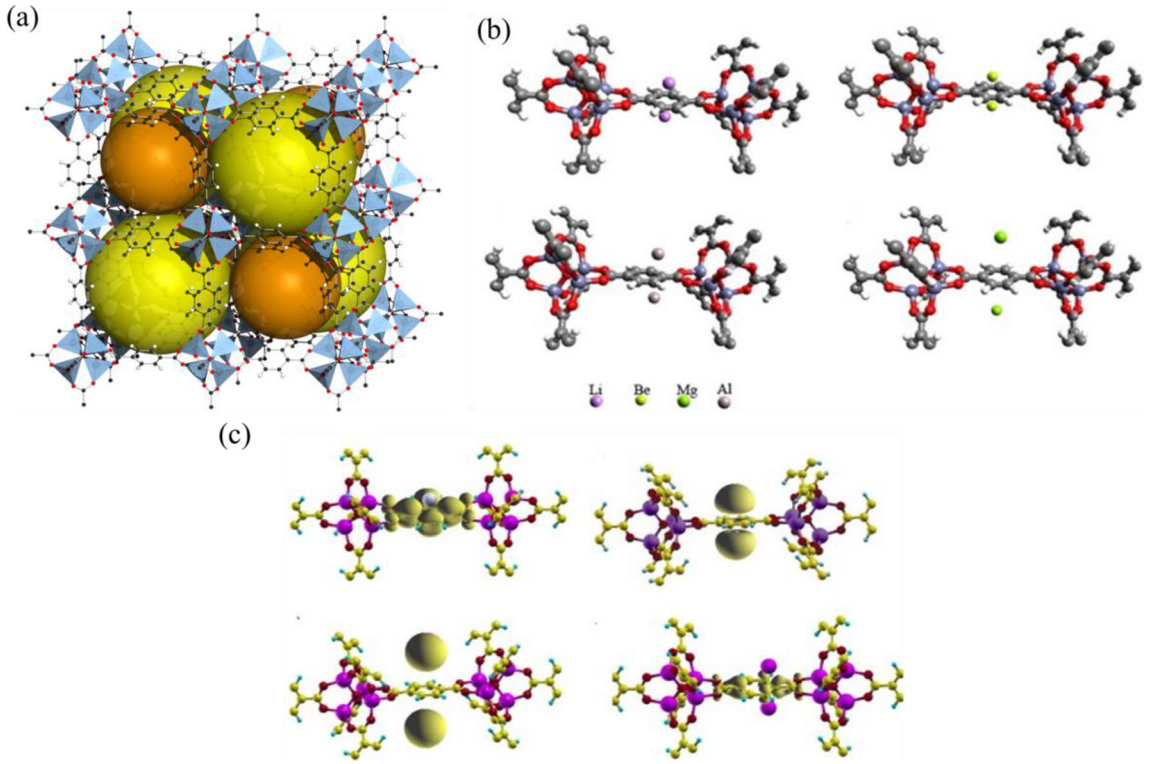

Figure 7. (a) The repeating unit of MOF-5*, (b) The optimized structures of Li-, Be-, Mg- and Al-decorated primitive cells of MOF-5** (c) Frontier molecular orbitals of metals and MOF-5**. *Reproduced with permission from Ref. 107. Copyright 2016 Wiley. **Reproduced with permission from Ref. 105. Copyright 2011 Elsevier.

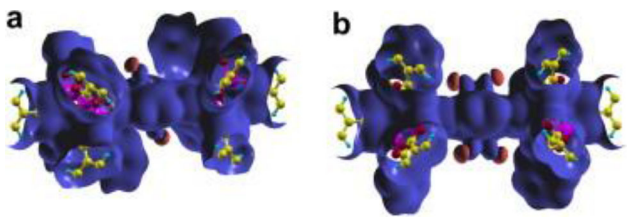

Figure 8. Charge density difference plots of (a) MOF-5:Li_2:$2H_2$ and MOF-5:Li_2 and $2H_2$ molecules and (b) MOF-5:Li_2:$4H_2$ and MOF-5:Li_2 and $4H_2$ molecules, at an isovalue of 0.01. Reproduced with permission from Ref. 105. Copyright 2011 Elsevier.

hydrogen molecules can efficiently interact with the metal cations. The Frontier Molecular Orbital approach was used to understand the attractive interactions as the HOMO and LUMO interactions are a better estimate for understanding reactivity. Among the light metals studied (M=Li, Be, Mg, Al), the Li- and Al-decorated MOF-5 has a HOMO which is of the p-character and was delocalized around the benzene rings and transferred electron density from metal to the organic linker (Figure 8).

The charge density was not delocalized in the case of Be and Mg, which are less suitable for enhancing H_2 adsorption in MOF-5. The suitability of the DFT functionals was tested by comparing the BSSE corrected binding energy for the BDC: Li_2:nH_2 molecular models using the MP2 level of theory and other DFT functionals in G09. The periodic calculations were performed using the PBE functional using the VASP. Among all the investigated functionals, the structural characteristics, atomic charges, and hydrogen binding energies were well estimated by the PBE method, which employs the plane-wave-based pseudopotential method. The computed gravimetric capacities and the higher H_2 binding energies obtained for Li and Al-decorated MOF-5 indicates that the Li- and Al-decorated MOF-5 will be adequate for storing H_2 at room temperature.[105]

Long and co-workers studied the effect of anion substitution in hydrogen adsorption in a family of M-BTT series MOFs $M_3[(M_4Cl)_3(BTT)_8]_2$ (M-BTT; M= Cu, Mn, Fe, Zn; BTT^{3-} = 1,3,5 benzenetristetrazolate).[103] The DFT model calculations were performed using the QChem[108] suite. Since the framework structure is periodic, the DFT calculations were carried out in a model complex, which contains a tetrameric unit of the primitive cell ($[M_4Cl(tz)_8]$) with four metal atoms bridged through chloride ligand and surrounding ligand is the tetrazolate moiety. Among the various functionals tested (LDA, BLYP, BP86, PBE, B3LYP, ω–B97, ω–B97X, ωB97X-D), the

ωB97X-D functional[109] yield accurate predictions for structural parameters, especially the metal and hydrogen distances (M = Mn, Cu)) and binding energy.

The binding energy was estimated by incorporating the basis set superposition error (BSSE) correction and accounted for the zero point energy under the harmonic approximation. The bond lengths and bond angles were calculated using the ωB97X-D functional for $[Mn_4Cl(tz)_8]$ and $[Cu_4Cl(tz)_8]$ are in good agreement with the experimental structures of Mn-BTT and Cu-BTT, corroborating the accuracy of the chosen functional.

Figure 9 depicts the structure of the tetrameric unit taken for the assessment of the H_2 binding energies (M = Mn, Cu, Zn; tz = 5-H-tetrazolate). The adsorption of H_2 was analysed in three different cases, in which the H_2 binding was observed in site I (near the metal center) or II (near anion) or the combination of both the sites. The binding energy for the hydrogen adsorption in the M-BTT series followed a Zn > Fe > Mn > Cu trend. Further, to check the role of anion substitution in hydrogen adsorption, the chloride ion was replaced with Br^- and F^- ions, and a case without any anions were also modelled. The substitution suggests that the size of the anion can affect the position of the metal center in the framework and, thereby, the strength of H_2 binding. The DFT investigations suggest that moving metal centres away from the plane of nitrogen atoms creates more accessible binding pockets for H_2, hence stronger electrostatic interaction of adsorbed H_2 molecules with the metal centres. Hence the trend of adsorption follows the order vacant site > $Br^- > Cl^- > F^-$. The possibility of Zn-BTT as a good H_2 storage device is also concluded in this work, emphasizing signs for the potential synthetic target for H_2 storage. The effect of substitutions of metal ion and anion of the tetrameric unit suggests that the configuration of this unit certainly plays a significant role in governing the affinity of the framework toward H_2.

Queen and co-workers reported a detailed investigation of molecular insight of hydrogen adsorption in a Cu-BTTri MOF possessing open metal sites through DFT methodologies combined with experiments.[110] The calculations were primarily concerned with exploring the different adsorption sites in Cu-BTTri ($BTTri^{3-}$ = 1,3,5 benzenetristriazolate) and their strength of hydrogen binding and associated structural properties featuring the same. The binding pockets in Cu-BTTri were obtained in four different positions in the framework. The site I is detected as the Cu center, and site II is between the hydrogen of the benzene ring and those of two nearby triazole rings. Site III is a pocket located between two nearby triazole rings, and site IV is the large pore of the framework facing the benzene rings. In all the sites, Van der Waal interactions play a key role in regulating the hydrogen binding energy and offer a way to enhance hydrogen binding in MOFs (Figure 10).[110]

The H_2-framework distance is estimated both experimentally and computationally, and the results were within an error bar of $\sim$0.2 Å. The D2 binding energies were calculated using PBE/DFT-D2 methods. The calculated binding energy for the site I is $\sim$10 kJ/mol and matches the experimental enthalpy of adsorption (10.5 kJ/mol). The calculations suggest that the net binding energy for the other three secondary sites is lower than that of site I, suggesting that site I will be the strongest.

Interestingly, the studies have also concluded that the alteration of the metal center is not changing the binding energy for hydrogen adsorption as the binding energy for the M-BTT series (M= Fe, Cr, Mn, Cu) ranged between 10.0 to 11.9 kJ/mol.[110] The study has provided a productive analysis of the minor effect of

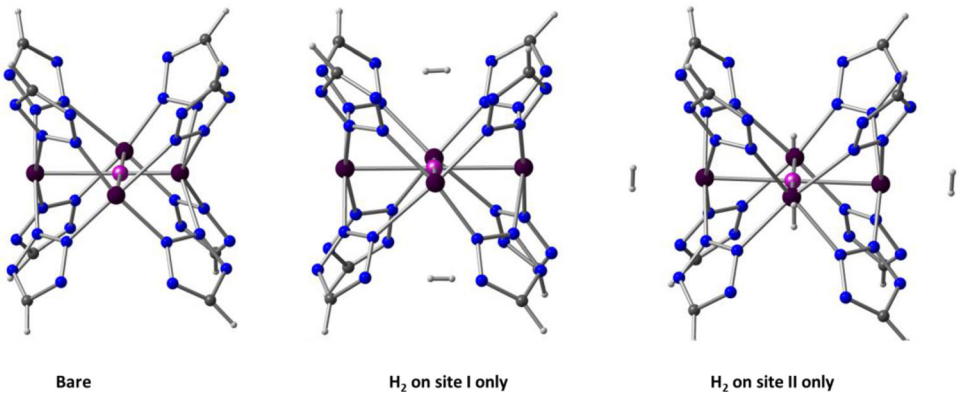

Figure 9. Structural model taken for MOF with added H_2 molecules with first at site I and then at site II. The M (M= Cu, Mn, Fe, Zn), N, Cl, C, and H are denoted as black, blue, purple, gray, and white, respectively.

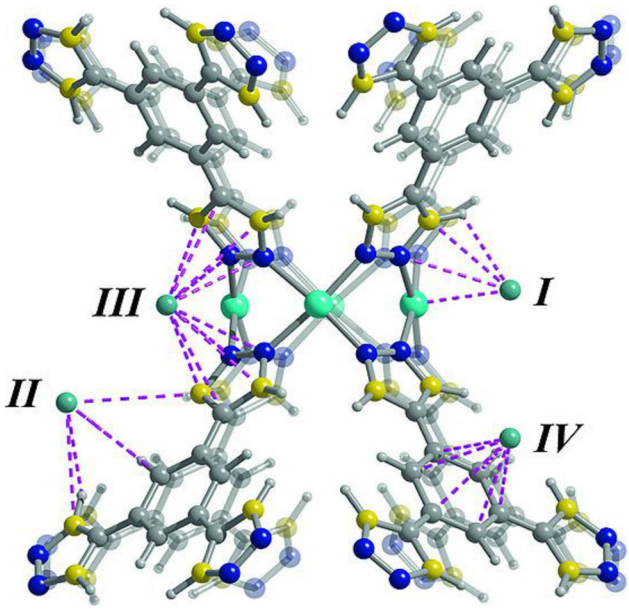

Figure 10. A ball and stick model of the Cu-BTTri framework dosed with 3.11 D2/Cu^{2+}. The Cu, C, N, and H are denoted as cyan, gray, blue, and white spheres, respectively. Yellow spheres represent mixed sites containing both C and N. The pink dotted lines represent nearest-neighbor interactions. Reproduced with permission from Ref.110. Copyright 2019 Wiley.

metal center alteration on the binding energy of site I. The energy decomposition analysis suggested a critical role of Van der Waal interaction in controlling hydrogen adsorption.

4. Modelling oxygen adsorption in MOFs

Oxygen is a crucial gas for the medical industry. During the Covid-19 pandemic, scarcity of O_2 was noticed in several countries as O_2/N_2 separation at the industrial scale currently utilizes cryogenic distillation, which is time-consuming and has a cost- and capital-intensive nature. Further, increasing carbon dioxide levels in the atmosphere have given researchers worldwide momentum to investigate this field, as high-purity O_2 is required for several post-carbon-dioxide captures.

A thorough investigation of the computational screening of MOFs for selective oxygen gas binding was conducted by Nenoff and co-workers in 2015.[111] They reported combined pDFT and experimental studies on $M_3(BTC)_2$ and $M_2(DOBDC)$ type frameworks (Figure 11a and 11b) where M= Sc, Ti, V, Cr, Mn, Fe Co, Ni Cu, Zn, Mo, Ru, Be, and Mg to look into the impact of metal in O_2/N_2 separations. The reliability of the DFT calculations was cross-verified by verifying the corresponding experimental binding energy trend for gas adsorption. The starting structures of $Fe_3(BTC)_2$,[112] $Cu_3(BTC)_2$,[74] $Fe_2(DOBDC)$,[113] $Co_2(DOBDC)$[73] $Ni_2(DOBDC)$,[114] $Zn_2(DOBDC)$,[115] and $Mg_2(DOBDC)$[116] were extracted from the literature. From the reported crystallographic structure data, the solvent and the water molecules were removed, and hydrogens were added for saturation. Apart from above mentioned MOFs, the rest of the structures were made by replacing the metal atoms in the corresponding model structures. The studies were carried out using PBE functional and DFT-D2 dispersion corrections with a 10^{-4} eV convergence threshold and force on each atom <0.03 eV/Å in VASP. The structural optimizations were accomplished with cut-off energy for plane waves of 500 eV and projector augmented-wave formalism, resulting in the cell length accuracy within 5% with experiments. The estimated binding energy for O_2 ranged from −354 to −21 kJ/mol and for nitrogen between −188 to −7 kJ/mol, and no relationship was found in-between binding energies and MOF structural type. The simulated binding energy is verified through examination of the experimental gas uptake at low-pressure and low temperature in $Cu_3(BTC)_2$, $Ni_2(DOBDC)$, and $Co_2(DOBDC)$. The 4d metals were found to have much higher binding energies than 3d metals, with the $Mo_3(BTC)_2$ being an exception. This is correlated to the nature of binding with the 4d ions have more diffuse 4d orbitals and can make a stronger affinity for oxygen than 3d metals. Also, it is correlated to the occupancy of the d-orbitals as the metal-oxo/superoxo/peroxo formation is correlated to the metal-O_2 back donation, which is likely to diminish as we move from 3d to 4d as the 3d-2p (O_2/N_2) gap is expected to be smaller than 4d-2p orbitals. Thus, late transition metals are not suited for O_2/N_2 because they bind O_2 and N_2 equitably. The MOFs of early transition metals having $M_3(BTC)_2$ and $M_2(DOBDC)$ framework structures were found to have oxygen binding that was substantially stronger than nitrogen binding. In particular, if synthetically feasible, $Sc_3(BTC)_2$, $Ti_3(BTC)_2$, $V_3(BTC)_2$, $Sc_2(DOBDC)$, $Ti_2(DOBDC)$, $V_3(BTC)_2$, $Cr_2(DOBDC)$, and $Mo_2(DOBDC)$ emerged as potential contenders for O_2/N_2 separation.

Apart from structural differences between $M_3(BTC)_2$ and $M_2(DOBDC)$ framework, the ability of a MOF to separate oxygen from nitrogen is determined by the kind of metal present in place of the type of framework structure. The fact that the binding energies for a particular metal between the two MOF topologies are very similar reveals that the ligands play a minor role in the O_2/N_2 separation (Figure 12).

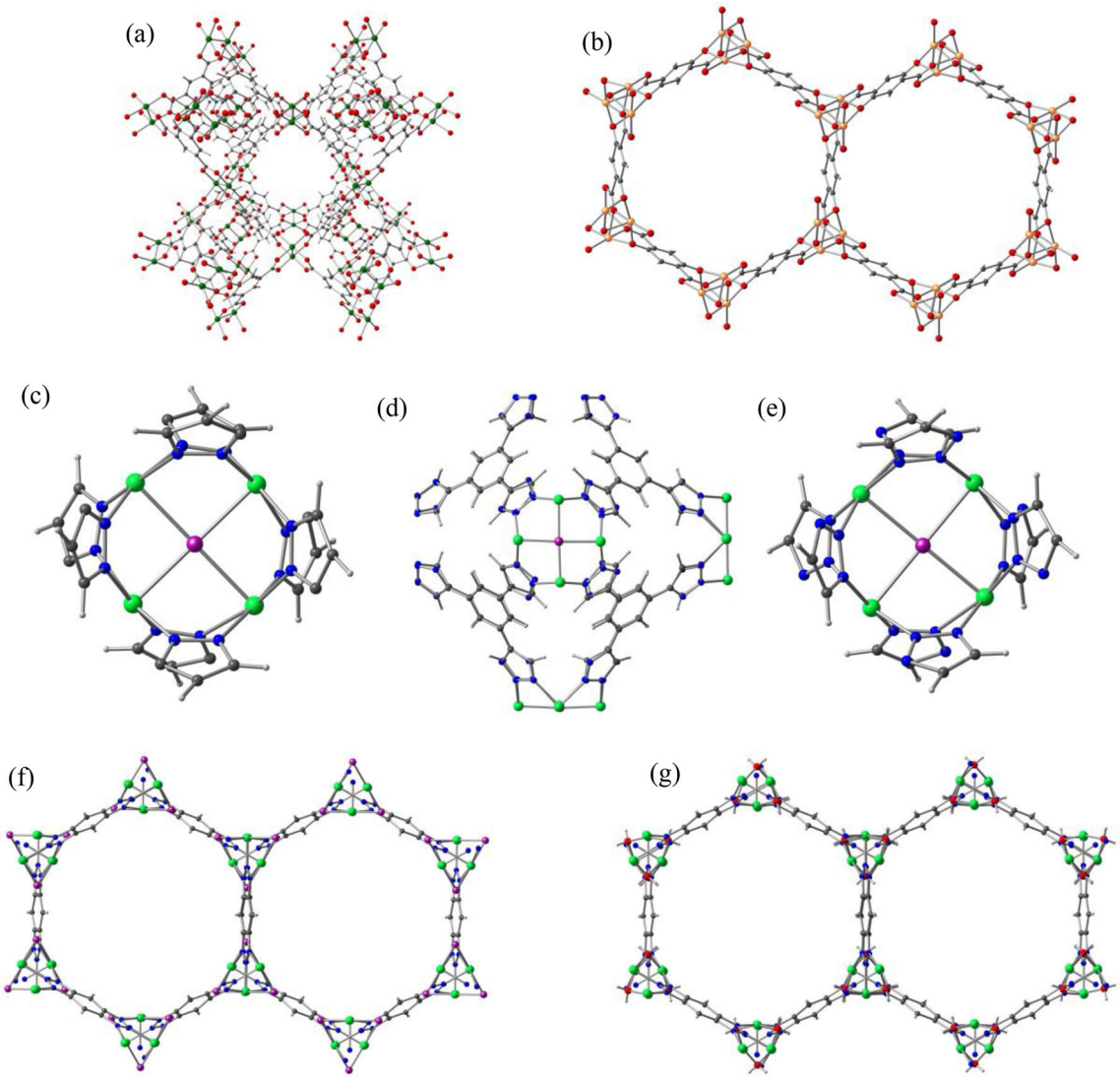

Figure 11. The representative MOF structures were chosen for the modelling studies of O_2 adsorption in MOFs, (a) Periodic unit of $Cr_3(BTC)_2$, (b) Periodic unit of $Fe_2(DOBDC)$, (c) tetrameric model of Co-BTTri, (d) Periodic unit of Co-BTTri, (e) tetrameric model of Co-BDTrip, (f) periodic unit of $Co_2Cl_2(BBTA)_2$,and (g) periodic unit of $Co_2(OH)_2(BBTA)_2$. The Cr, Fe, Co, N, Cl, O, C, and H are denoted as dark green, orange, light green, blue, purple, red, gray, and white, respectively.

However, a year later, a work by Long and co-workers examined the effects of linkers on oxygen binding in a Co-based metal-organic framework.[50] This study performed thorough electronic structure calculations combined with experimental synthesis and analysis. Among the two cluster models chosen, the first model, a tetrameric unit ($[Co_4Cl(Tri)_8]^{1-}$ HTri =1,2,3-triazole) was considered (Figure 11c). The M06 functional was employed with an all-electron basis set def2-TZVP in the Gaussian 09 suite for DFT calculations. For deeper insights, multi-configurational calculations were carried out on unbound as well as O_2-bound complexes using the full active space self-consistent field (CASSCF) approach and subsequent advancement second-order perturbation theory (CASPT2) in the MOLCAS 8.0 suite.[117] In this second cluster model, pDFT calculations were carried out in the VASP suite using gradient-corrected PBE functional, including Grimme's D3 dispersion correction. (Figure 11d). A plane-wave energy cut-off of 400 eV with a 10^{-5} eV convergence threshold and force on each atom within 0.05 eV/Å were employed. To examine how the various ligands affect the Co-O_2 binding, authors have also performed cluster model calculations for Co-BTT and Co-BTP systems. The ground state of the $[Co_4Cl]^{7+}$ node is projected by the DFT, CASSCF, and CASPT2 approaches for the activated framework and is consistent with experimental results (Figure 13).

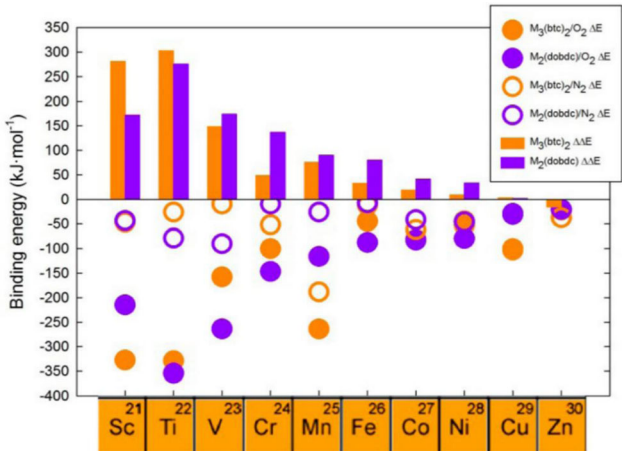

Figure 12. The difference in binding energies (ΔΔE) between oxygen and nitrogen binding (bars) and binding energies for nitrogen (open circles) and oxygen (closed circles), for variants of $M_3(BTC)_2$ (orange) and M_2-(DOBDC) (purple) containing first-row transition metals. Reproduced with permission from Ref.111. Copyright 2015 American Chemical Society.

Based on the results of M06 functional, each Co^{II} centre's spin density indicates a small degree of oxidation which occurs upon oxygen binding. Approximately ~0.25 electrons were transferred from cobalt to O_2, and this modest charge transfer was further supported by the CASSCF multi-configurational wave function partial occupation number (0.20 electrons). The experimental measurement of 34(1) kJ/mol is within the error of the DFT- estimated enthalpy of adsorption of oxygen, which is 32.8 kJ/mol by M06 functional (Table 2). The Co-BTTri displays low binding energy, and hence, less selectivity is seen for this framework, along with low oxygen adsorption. So, the authors tune the ligand and synthesised H_3BDTriP (5,5′-(5-(1H-pyrazol-4-yl)-1,3-phenylene)bis(1H-1,2,3-triazole)) having Brunauer–Emmett–Teller (BET) surface area of 1332(4) m^2/g for checking the effect of changing ligand on selectivity. Although Co-BDTriP and Co-BTTri have fairly comparable O_2-dosed crystal structures, a subjective assessment of the slopes of their oxygen isotherms showed that Co-BDTriP had a substantially larger propensity for O_2. The Co-BDTriP displayed greater oxygen affinity along with smaller isosteric heat for N_2 at lower loadings. This, in turn, results in a better O_2/N_2 selectivity because of the weaker Lewis acidity of pyrazolate-bound metal centres.

Using DFT calculations, isostructural organic linkers can fine-tune the selectivity, the heat of adsorption, and electronic structures, oxygen binding was thoroughly studied in the isostructural frameworks Co-BTT, Co-BTTri, and Co-BTP. The bond lengths of Co-O, Co-N, and Co-Cl decrease in the order Co-BTT followed by Co-BTTri, which in turn is greater than Co-BTP and this is reversed if we compare the amount of charge transfer from metal to O_2. Based on these results, the authors have speculated that Co-BTP could be fascinating for applications involving higher-temperature air separation and aerobic oxidation catalysis. The authors have proved that considerably adjusting the ligand field modifies the O_2 heat of adsorption and the amount of electron transfer from Co to O_2 and have shown that a judicious choice of both

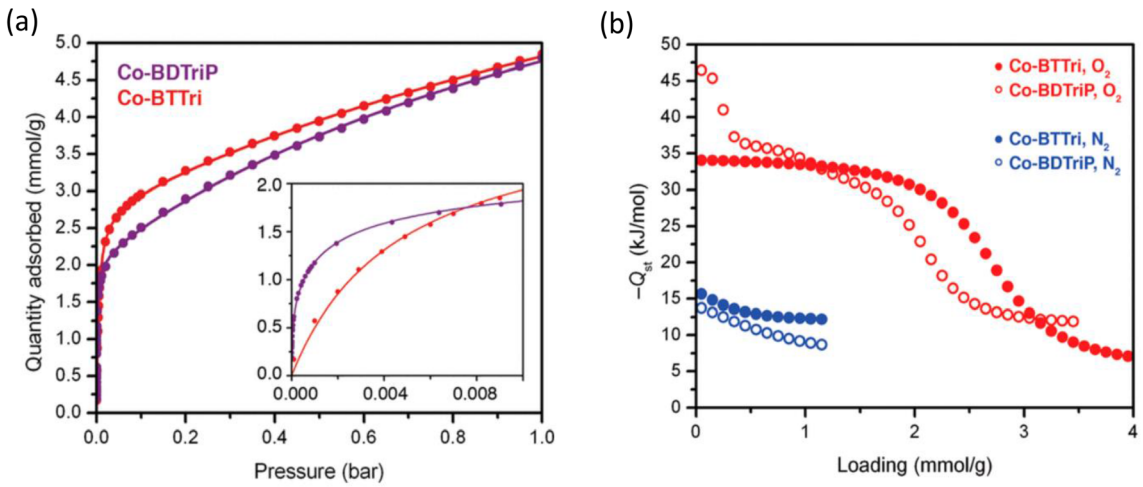

Figure 13. (a) Comparison of O_2 adsorption isotherms collected for Co-BTTri (red) and Co-BDTriP (purple) at 195 K. Filled circles and solid lines represent experimental data, and their corresponding Langmuir fits, respectively. Inset: Low-pressure region of 195 K O_2 isotherms. The Co-BDTriP–O_2 uptake is significantly steeper at these low pressures than Co-BTTri. (b) Comparison of Co-BTTri (filled with red and blue circles, respectively) and Co-BDTriP (open red and blue circles, respectively) O_2 and N_2 isosteric heats. Reproduced with permission from Ref. 50. Copyright 2016 American Chemical Society.

frameworks as well as the ligand field is important for obtaining higher selectivity. However, the work on M_2(DOBDC) discussed earlier underestimated the role of MOF topology and attached a prime role for the nature of the metal ions. Though Co-BTTri and Co-BDTriP showed appreciable selectivity and can adsorb O_2 reversibly over N_2, their selectivity is dramatically diminished at temperatures beyond 195 K.

As a large number of nodes and linkers are available in the MOF literature, there is a requirement for design criteria that could be applied to effectively adjust the oxygen and nitrogen affinities at frameworks exposed metal locations because it takes a significant amount of time to create, characterise, and test novel MOFs for O_2/N_2 separation. Here, the work of Snurr and co-workers[118] holds importance. Here the VASP package with projector-augmented wave (PAW) pseudopotentials, convergence criteria of 10^{-6} eV, the force acting on every atom within 0.03 eV/Å, and cut-off energy of 520 eV was employed to compute adsorption energies for the DFT calculations, with PBE-D3(BJ) theory level. The refinement of atomic locations was carried out with M06-L meta-GGA exchange-correlation functional with fixed lattice constants. All further computations concerning the adsorption of any guests were performed using a constant simulation unit cell employing M06-L functional. Adsorption of oxygen and nitrogen at unsaturated metal locations was explored for different families of MOFs using a screening technique based on pDFT. The authors aim to design procedures to tune the redox activity of the MOF-metal centers by altering the formal oxidation states, anions of bridging coordination entities, and functionalisation of the linkers to change the O_2 selectivity at open metal spots. The authors examined O_2 and N_2 adsorption at the open metal sites of different MOF types using a high-throughput pDFT approach. In order to recognise structure-property associations which could be utilised to inform the outline for MOFs having greater selectivities for oxygen at open metal sites, authors have precisely chosen some MOF families which are structurally related. These include $M^{(II)}{}_2$(DOBDC), $M^{(II)}{}_2$(DSBDC), $M^{(II)}{}_2Cl_2$(BBTA), (H_2BBTA =1H,5H-benzo(1,2-d:4,5-d′)bistriazole), $M^{(II)}{}_2(OH)_2$(BBTA), and $M^{(II)}M^{(III)}{}_2$. For M^{2+} position V^{2+}, Cr^{2+}, Mn^{2+}, Fe^{2+}, Co^{2+}, Ni^{2+}, Cu^{2+}, and Zn^{2+} ions were considered, and for M^{3+} position Sc^{3+}, Ti^{3+}, V^{3+}, Cr^{3+}, Mn^{3+}, Fe^{3+}, Co^{3+}, and Ni^{3+} ions were considered. The authors predicted that the isostructural framework [$Co_2(OH)_2$(BBTA)] formed by replacing the bridging Cl^- ligands of [Co_2Cl_2(BBTA)] with OH^- could enhance the O_2 selectivity.

The fact that $Co_2(OH)_2$(BBTA) demonstrated a value of ΔH_{O_2} = 45 kJ/mol and [Co_2Cl_2 (BBTA)] a value of ΔH_{O_2} = 19 kJ/mol proved that prediction is supported experimentally, and hence, indicates that open-metal sites possessing MOFs which are usually redox active could be made to adsorb oxygen. As $Co_2(OH)_2$(BBTA) binds O_2 more strongly, this shows that similar kinds of MOFs would be effective for reactions that require the presence of redox-active centers.

Based on stark differences in O_2 affinities for Co_2Cl_2(BBTA) and $Co_2(OH)_2$(BBTA), the authors anticipated that the post-synthetic ligand exchange method is an assuring technique for improving the O_2 binding tendencies. According to the studies, it was clear that the acidic strength of bridging anion also affects the degree of oxygen adsorption, and it concluded that a ligand with a higher pKa value would lead to a more redox-active metal site. They also accomplished that the potency to bind oxygen is a consequence of the amount of charge transferred. Keeping up with the above observations, early TMs associate O_2 strongly in low oxidation states as they would have easily oxidisable metal centers.

Although various explorations have been carried out for the improvement of MOFs for gas adsorption in various manners, such as the modification of bridging linker parts, ligands, and metals, very few studies have been undertaken to unveil the role of spin state and spin coupling properties of oxygen binding. Based on the CSD database analysis (Figure 1), it is clear that most of the reported MOFs are paramagnetic, and it is of great relevance to tune the spin state and spin coupling for gas adsorption.

In this context, we have reported the decisive role of the magnetic coupling of MOFs in controlling selective oxygen binding compared to other gases such as hydrogen and nitrogen.[119] The pDFT calculations were performed in a coordinatively unsaturated $Cr_3[(Cr_4Cl)_3(BTT)_8]_2$ (Cr−BTT; BTT^{3-}=1,3,5-benzenetristetrazolate) unbound MOF and gas-bound Cr-BTT MOF ($([(Cr_4(X_2)_4Cl)_3(BTT)_8]^{3-}$), X=$O_2/N_2/H_2$) (Figure 14a). This MOF demonstrates an impressive preference for O_2 over N_2/H_2. Here we have employed the CP2K suite with PBE functional with a Gaussian Augmented Plane Wave (GAPW) approach having a kinetic energy cut-off of 400 Ry. The calculations were performed incorporating both Grimme's D2 as well as D3 dispersions, and it was found that D3 calculations were yielding better results.

The simulations of the adsorption isotherms were performed using RASPA software[120] employing the

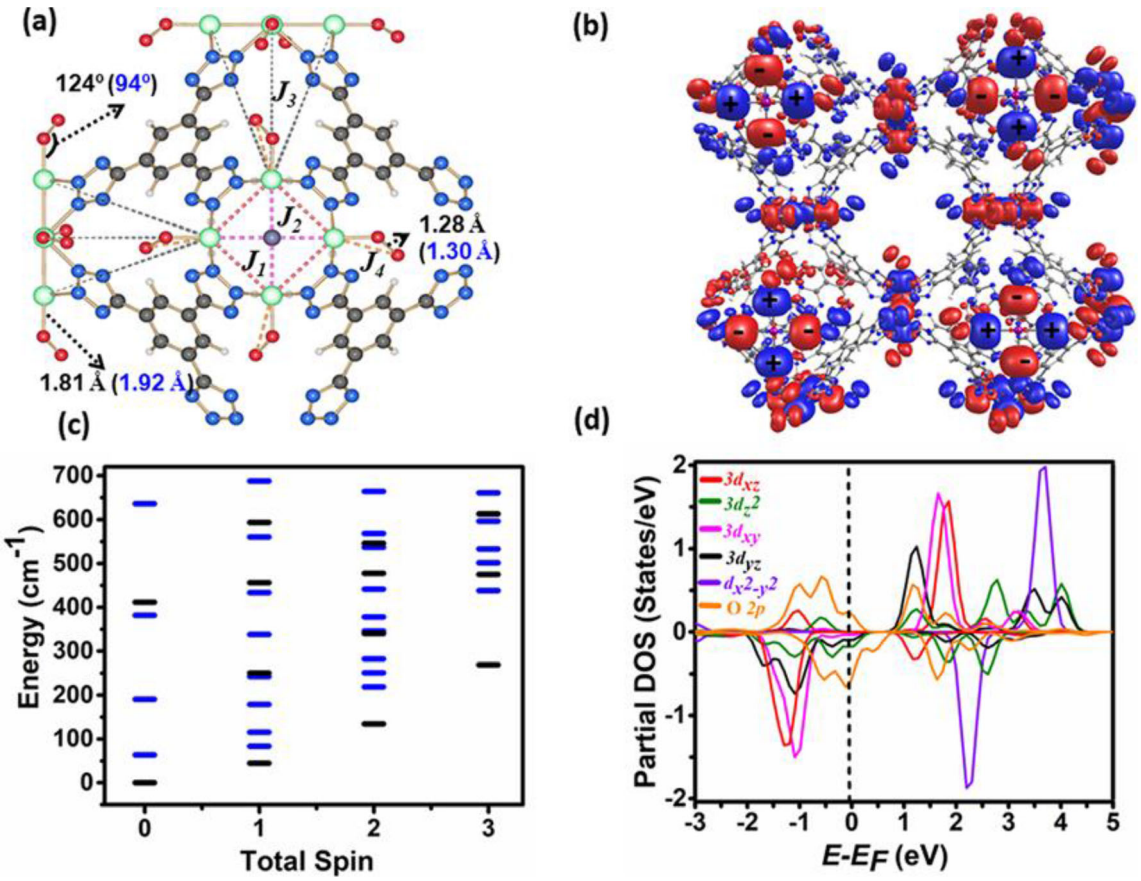

Figure 14. (a) Geometry and representation of $J_{1–4}$, bond parameters of GS (in black) and HS in $[(Cr_4(O_2)_4Cl)_3(BTT)_8]^{3-}$ MOF. (Cr: green, Cl: purple, N: blue, C: gray, H: white). b) GS spin-density plot of $[(Cr_4(O_2)_4Cl)_3(BTT)_8]^{3-}$. c) Estimated spin-state ladder based on DFT J values for O_2-bound (black) and unbound MOF. d) The partial DOS plot for the $[(Cr_4(O_2)_4Cl)_3(BTT)_8]^{3-}$ MOF. Reproduced with permission from Ref. 119. Copyright 2020 Wiley.

Grand Canonical Monte Carlo technique. Lorentz-Berthelot mixing rules are utilized to determine the cross interactions for the framework atoms under consideration. The Lennard-Jones (LJ) values for these atoms were acquired from the Universal Force Field (UFF).[121,122] The optimization of the unbound Cr-BTT suggested a diamagnetic ground state of the system with an S=0 spin state, where the spin-spin states of the chromium atoms in tetrameric units were aligned in spinup-up-down-down configurations (Figure 14b). Upon binding of oxygen, the alignment of diamagnetic ground spin states was found to be in spin up-down-up-down configurations.

Whereas in the case of hydrogen and nitrogen adsorption, the magnetic ground states remained unaltered, suggesting that the O_2 adsorption can be tuned using different spin states. The investigation of O_2 binding suggests that the redox mechanism occurs in the framework to accommodate oxygen as superoxo species, and Cr^{II} is converted to Cr^{III}, whereas the H_2 and N_2 were not forming such a radical anion species. Further, the exchange coupling constants in the bound and unbound Cr-BTT were estimated.

The framework has mainly three J values, where J_1 is mediated between the nearby chromium centers connected through the nitrogen of the BTT ligand, J_2 is mediated between two chromium atoms which are bridged by chloride linker, and J_3 is the interaction between adjacent tetrameric units which are connected through BTT ligand (Figure 14a). The binding of O_2 gives rise to an additional J value which is mediated *via* the Cr^{III} centers and superoxo radicals. The estimated J values for unbound and O_2 bound Cr-BTT is J_1=-25.8 (-23.8) cm^{-1}, J_2= -41.8 (+3.4) cm^{-1} and J_3 = 0.3 (+0.5) cm^{-1} (J_4 = -1366 cm^{-1}), which is suggesting a change in value of J_2 after binding of O_2. The ground state configuration of chromium has a spin density of ~2.9 (~3.8 on unbound MOF) and oxygen, ~0.9. The calculations suggested that the electron-transfer mechanism adopted by O_2 gives rise to Cr^{III} superoxo species ($O_2^{\cdot-}$) with a very strong antiferromagnetic coupling between the two centers.

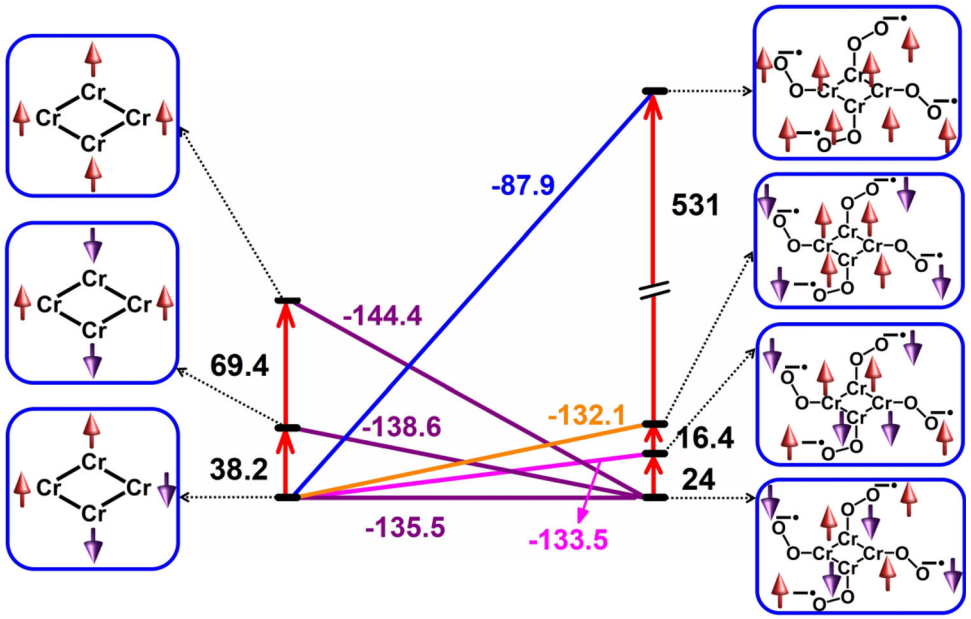

Figure 15. The energy level diagram depicts different spin states comparative energies [kJ/mol] before and after oxygen binding. Reproduced with permission from Ref. 119. Copyright 2020 Wiley.

This stabilizing exchange coupling interaction between Cr^{III} centers and oxygen leads to spin-state-dependent binding. Further, the oxygen binding in various spin states like high spin, intermediate spins, and ground states was examined (Figure 15). Interestingly, the binding energy of high spin and ground state differed by ~47 kJ/mol, which suggests strong spin-state dependent oxygen binding. The successive oxygen binding and analysis of binding energy in various spin states corroborate the fact that the number of bound oxygen and the value of binding energy varied in the ground state and high spin state (Figure 16c). The adsorption trend for H_2/N_2 was similar in both high spin and ground states. This was also cross-verified by classical adsorption isotherm simulations where GS and HS have different adsorption capacities (Figure 16a,b). The isotherm calculations were performed by considering the successive oxygen binding and capturing their uptake capacities. Up to eight oxygen binding, the isotherm matched with the experiments in the case of the ground state. In contrast, the adsorption isotherm for other H_2/N_2 did not show any change in the isotherm pattern and followed a similar isotherm profile, both in high spin and ground state. Thus the adsorption isotherm calculations also demonstrate no spin-dependent binding for H_2/N_2 (Figure 16b). Further, to cross-check if any radical formation occurs upon binding of nitrogen, a coordinate scan was performed to access the energetic cost associated with the radical formation of N_2. The calculations suggested the formation of Cr(III)-$N_2^{-\bullet}$ species at N-N ~1.34 Å, with an energy penalty of ~150 kJ/mol (per site), revealing the reason for the very high selectivity towards O_2 (Figure 16d). This study offered a hitherto unexplored method of controlling gas adsorption selectivity in MOFs by applying spin-state/spin-coupling switching.

5. Modelling methane adsorption in MOFs

The major problem chemists face nowadays is the safe storage of energy. There is great interest in storing and recovering methane as it burns cleanly compared to other conventional fuels like gasoline and has a greater H/C ratio. The fact that condensed methane's volumetric energy density is just 1/3rd of gasoline is a massive disadvantage. Therefore, there is a demand for better methane storage materials. The U. S. Department of Energy (DOE) established a benchmark for material-based adsorption of CH_4 storage, in 2000, of 180 cm^3(STP) cm^{-3} at 298 K and 35 bar to motivate research in this area. Traditional adsorbent materials like zeolites show a value within 100 cm^3 (STP) cm^{-3}, carbon-based materials reasonably meet this value, but there is not enough room for better performance due to finite surface area. MOFs are of interest as they have already surpassed this value and are present in the literature, and a further improvement in the surface area can be made because of their tunable nature.

Molecular Simulation is vital in screening existing and hypothetical MOFs for any particular applications. For methane adsorption, Sanyue Wang,[123] in 2007,

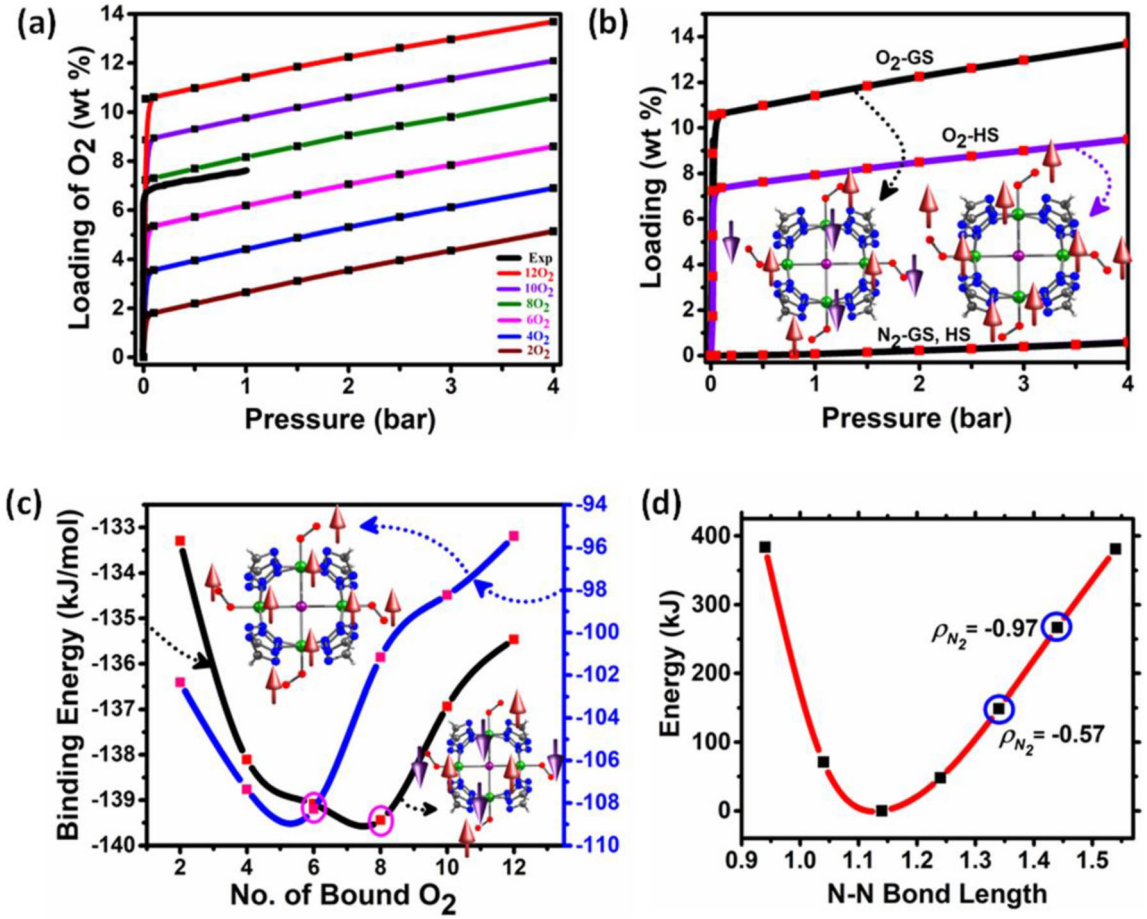

Figure 16. (a) Computed adsorption isotherm for successive O_2 binding. b) Comparative adsorption isotherm for O_2 and N_2 in GS and HS states. c) Computed BE for successive addition of oxygen in GS (black, *S*=0) and HS (blue) states. d) Rigid scan of N−N bond distance in N_2-bound MOFs. Here the blue circled regions indicate the formation of radical at the N_2 moiety and corresponding spin density. Reproduced with permission from Ref. 119. Copyright 2020 Wiley.

simulated a series of 10 MOFs utilizing Monte Carlo simulation to evaluate the required properties of an idyllic adsorbent. The guest-free microporous frameworks Cu-BTC, CPL-2, CPL-5, $Cu(AF_6)(bpy)$, and IRMOFs (1, 6, 8, 10, and 14) were used for simulations, and their structures were modelled employing Materials Studio Visualizer from X-ray diffraction (XRD) data. In this work, authors employed Lennard-Jones (LJ) site interactivity simulation to explain the CH_4 gas adsorption. Using the transferable potentials for phase equilibria (TraPPE) force field, the prospective considerations of σ_{CH_4} = 0.373 nm, ε_{CH_4}/k_B = 148.0 K were taken for the CH_4 molecule. To know the association between atoms of the framework and methane molecule, all-atom optimized potentials for liquid simulations (OPLS-AA)[124] force field was utilized. Adsorption of CH_4 across all frameworks was calculated using the conventional Grand Canonical Monte Carlo (GCMC) simulations. Rigidity was considered during simulations in all MOFs. For LJ interactions, a cut-off radius value of 13.5 Å was employed with periodic boundary limits in all directions. The simulation used 10^7 iterations for each state point to ensure equilibration and 10^7 iterations to model the appropriate thermodynamic characteristics. The maximum overall potential energy and the ensemble average in the simulation cell are predicted to have an error of around 2% on the final results. Chemical potentials were computed from the NPT ensemble MC simulation. On the grounds of the simulated chemical potentials at different pressures, relationships between chemical potentials and pressure were built to convert them into each other. Simulations suggest that for methane storage, an ideal absorbent would be one with a specific surface area, low density, superior isosteric heats of adsorption, and free volume. With the comparison between methane uptake values in various MOFs considered, authors found the role of various factors in methane adsorption. They draw the inference from these simulations that the free volume and accessible surface area are crucial in determining the absorption of methane at 3.5 MPa and 298 K conditions. This study proved molecular simulations are

a valuable tool to decipher adsorption capacity. This, in turn, directs rules for the design of novel materials. However, this study does not involve any quantum chemical calculations; thus, it completely ignores the role of open-metal centers and possible chemical bonding between the metal and the gas, as seen in earlier studies. The method used by authors in this study can only predict adsorption in frameworks which does not have strong binding sites. The above method is not sufficient enough to take into account the strong gas/framework interactions.

The function of open-metal sites was later explored in 2009 by Yildirim and co-workers.[70] Even though the CH_4 molecule is nonpolar and extremely symmetric, some increase in binding energy is feasible because the distribution of charges on the CH_4 molecule would change as a result of adsorption on the metal location. Thus, symmetry would be reduced, resulting in the formation of multipole moments. Authors explored the M_2(DHTP) family of MOFs (Figure 17a-d), which contains large volumes of unsaturated metal sites (where DHTP= 2,5-dihydroxyterephthalate and M = Mg, Mn, Co, Ni, and Zn). They found that the adsorption of a single methane molecule per site can produce a significant CH_4 storage capacity of about 160–174 cm^3(STP)/cm^3, reaching the objective set by DOE of 180 cm^3(STP)/cm^3 for CH_4 storage in materials at ambient temperature conditions. The authors computed adsorption and desorption isotherms at 270, 280, and 298 K on five activated M_2(DHTP) samples with the modified Clausius–Clapeyron equation and determined the heats of CH_4 adsorption. Excess methane uptake capacity for the five M_2(DHTP) varies from 149 to 190 cm^3(STP)/cm^3 at 35 bar and 298K. This matches well (within 10%) with these MOFs' (Table 2) predicted largest uptake tendencies at open-metal sites. The largest methane storage capacity among MOFs under investigation is Ni_2(DHTP), with an adsorption capacity in absolute terms of roughly 200 cm^3(STP)/cm^3, potentially exceeding the DOE goal by about 10%.[70]

DFT calculations were performed using the Plane-Wave Self-Consistent Field (PWSCF) code to determine the binding energy of methane molecules at unsaturated metal sites. They investigated LDA and PBE functionals using Vanderbilt-type ultrasoft pseudopotentials with a cut-off energy value of 544 eV and overall energy convergence within 0.5 meV/atom. Based on the above calculations, the B.E of methane at open metal sites was found to be much higher than at any other sites. It was also reflected in the high heat of adsorption for CH_4 in these MOFs. They considered that the electrostatic associations among methane and open metals are responsible for the increased binding strength. However, in this work, the role of cage opening for the methane entering the framework was not explored.

One year later, in 2010, Zhou and co-workers[125] revealed that small cages/channels are also important in methane storage. The authors published a thorough mechanistic analysis of CH_4 storage in three landmark MOFs, HKUST-1 [Cu_3(btc)$_2$] (btc=1,3,5-benzenetricarboxylate), PCN-11 [Cu_2(sbtc)] (sbtc=trans-stilbene-

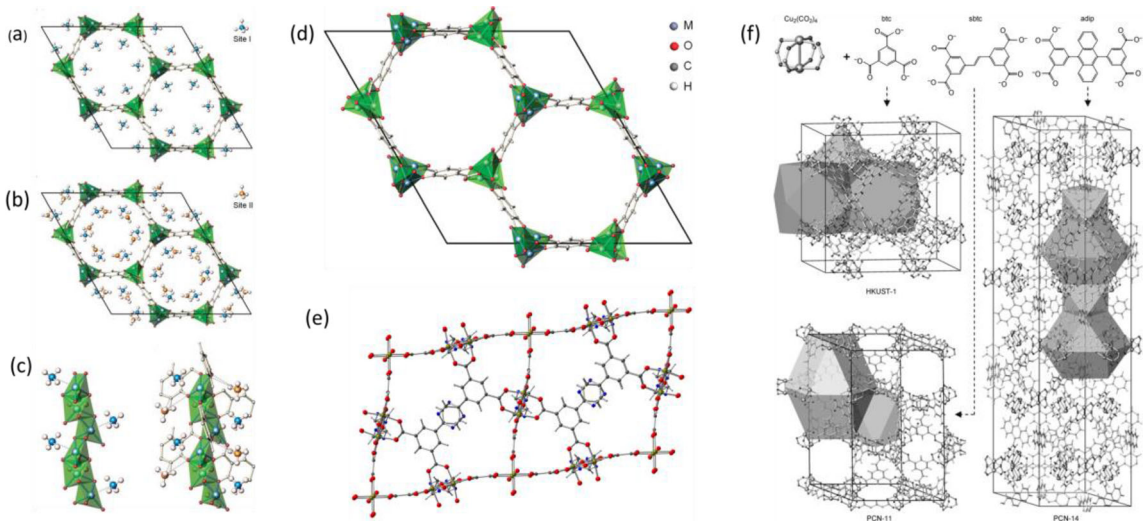

Figure 17. The representative MOF structures are taken for the investigation of CH_4 modelling studies in MOFs, (a-c) different binding sites in Zn_2(DHTP)*, (d) bare structure of the Zn_2(DHTP)*, (e) UTSA-76a, and (f) Crystal structures of HKUST-1, PCN-11, and PCN-14**. * Reproduced with Permission Ref. 70. Copyright 2009 American Chemical Society, ** Reproduced with Permission Ref. 125. Copyright 2010 Wiley.

3,3′,5,5′-tetracarboxylate), and PCN-14 [Cu_2(adip)] (adip=5,5′-(9,10-anthracenediyl) diisophthalate)) (Figure 17f) through neutron powder diffraction trials, followed by GCMC simulations and DFT computations to know the precise positions of methane molecules deposited in these frameworks. The Rietveld refinement's of experimentally determined positions and the relative numbers of the adsorbed CH_4 at each major binding site (apart from unsaturated metal positions) are in good agreement with those anticipated by GCMC simulations. Smaller cage openings and unsaturated Cu sites in HKUST-1 have a higher occupation, while the primary centre location of the small cages and corner location of larger cages are sparsely occupied. The fact that experimental findings and the results from the GCMC simulation are qualitatively consistent leads authors to believe the conventional force fields they employed can seize the main vdW-type interplay among methane and the MOF framework. DFT calculations provided additional support for the experimentally observed structures of adsorbed methane. The DFT optimizations for adsorbed CH_4 in HKUST-1 and PCN-11 were found to be entirely consistent with the outcomes of the experiment. The PWSCF software was used to carry out DFT-based computations using LDA with the Perdew-Zunger (PZ) exchange-correlation functional and ultrasoft Vanderbilt pseudopotentials, with an energy cut-off of 544 eV with convergence within 0.5 meV per atom was employed. The binding between methane and open metal position is underestimated by GGA approximation; therefore, it was not employed in this study. The authors summarised the experimental values of primary adsorption enthalpy and static methane binding energies derived by DFT for all adsorption sites. The binding capacity of CH_4 is overestimated by LDA approximation resulting in significantly higher adsorption enthalpies compared to experimental values. Authors discovered that there were two main types of strong adsorption sites where methane uptake occurs: (i) one at coordinatively unsaturated Cu sites, which show better Coulomb interactions with CH_4, and (ii) the second at the sites having potential van der Waals pockets. It is interesting to note that the improved van der Waals locations are only found in smaller cages. On the other hand, CH_4 binds very little to larger cages having even pore overlays. These findings imply that rational novel MOF compound development for CH_4 stowage purposes must concentrate on increasing the number of open metal sites, limiting the proportion of larger pores, and raising the proportion of available small channels and cages.

Later, in 2014, Banglin Chen and co-workers[126,127] found a new MOF, "UTSA-76a" (Figure 17e), which had dynamic pyrimidine groups on the linker. It showed an extremely high CH_4 uptake of about ~260 cm^3 (STP) cm^{-3} at 65 bar and 298 K, which is much greater than the target value of DOE. The authors calculated the storage capacity of methane in UTSA-76a, and it was contrasted with NOTT-101a. UTSA-76a showed significantly more methane adsorption besides NOT-101a at 298 K and 65 bar. The capacity to store volumetric methane significantly increased from 237 cm^3 (STP) cm^{-3} (NOTT-101a) to 257 cm^3 (STP) cm^{-3} (UTSA-76a). The elevated working capacity and methane storage observed in UTSA-76a implied that the immobilization of functional groups into pore surfaces of MOFs plays a significant role in the markedly enhanced methane storage performance. They thoroughly analyzed UTSA-76a and NOTT-101a from a skeletal standpoint by neutron scattering and computational studies to comprehend the cause of the greater uptake of CH_4 by the pyrimidine groups. They looked into the possibility that the CH_4 adsorption energies in these MOFs would be distinct and lead to the differences in methane adsorption isotherms. They used van der Waals (vdW) corrected interactions employing dispersion-corrected density-functional theory (DFT-D) computations. Observations showed that the binding energies of adsorbed methane molecules on the primary phenyl ring of NOTT-101a and those close to UTSA-76a's pyrimidine sites are comparable. Comparing UTSA-76a to NOTT-101a, they did not observe any novel, particular adsorption sites that had been brought by the pyrimidine rings. The DFT-D estimated adsorption affinities on the surface of the organic linker pore were virtually comparable to these MOFs' static structures and unable to explain the variation in methane storage capacity, which prompted them to think about the dynamic structure of these frameworks. However, researchers observed that the center linker's rings have rather high freedom of rotation, which might have some impact on methane storage. Thus, the energy required for this rotating movement about two corresponding configurations of the core rings was computed, in which they discovered that the central linker's ring of NOTT-101a is substantially more "static" than the central linker's ring of UTSA-76a as it possesses higher rotational barrier. They observed that UTSA-76a has a substantially lower estimated barrier for rotation of the benzene group than MOF-5 (55 kJ/mol). Therefore, compared to the central benzene rings in NOTT-101a, in order to maximize the methane packing at elevated pressures during methane adsorption, UTSA-76a's central

pyrimidine rings could be easily altered and directed. As a result, both MOFs exhibit almost the same uptake at low pressures. However, with larger methane loadings, due to its flexible orientation of the pyrimidine ring, UTSA-76a is capable of adsorbing greater gas molecules compared to NOTT-101a, giving it a larger working capacity. This study revealed that MOFs with comparable dynamic linker freedom could provide greater CH_4 working and storage capacities.

6. Modelling mixture of gas adsorption in MOFs

In 2014, Jeffrey B. Neaton and coworkers,[128] employing density functional calculations, calculated and examined 14 distinct small gases binding enthalpies, including H_2, CO, CO_2, H_2O, H_2S, N_2, NH_3, SO_2, CH_4, C_2H_2, C_2H_4, C_2H_6, and C_3H_8, in M-MOF–74, a family of MOFs where M = Mg, Ti, V, Cr, Mn, Fe, Co, Ni, Cu, and Zn. This research made statistical inferences that improved our knowledge of the role of different transition metal cations in small molecule binding at coordinatively unsaturated metal locations and pinpointing promising candidates for gas-separation applications. Due to flaws in correlation and self-interaction, traditional exchange-correlational functionals, like LDA or GGA, may not accurately describe localized *d* electrons. The fact that adsorption energies are significantly influenced by vdW dispersion interconnections among small gas molecules and MOFs and thus create a nonlocal correlation is typically ignored by local or semi-local exchange-correlational functionals. The authors employed vdW-DF2 with Hubbard U corrections for the d electrons of the transition-metal ions to resolve these issues as vdW-DF2 had displayed in the literature to reproduce appreciable values for smaller molecules. They evaluated the efficacy of their method by contrasting their findings with those obtained through measurements of MOF-74s' electronic structure, lattice characteristics, and isosteric temperatures of CO_2 adsorption. All computations are performed using the VASP suite employing PAW pseudopotentials and a plane-wave basis set with a high plane-wave cut-off energy of 1000 eV and binding energies that converge within one kJ/mol. They started with known Zn-MOF-74's established structure. Employing PBE functional, a triclinic primitive unit cell was modelled and utilized to produce the Zn-MOF-74's structure. Optimization of atomic locations and lattice vectors was performed till the stress tensor components were less than 0.2 kbar, and residual forces were less than 0.01 eV/Å. Swapping out the Zn atoms for Mg, Ti, V, Cr, Mn, Fe, Co, Ni, and Cu creates isostructural analogues with different metal cations. These new structures are then re-optimized employing PBE functional having Hubbard corrections. The apical M-O bonds in Cr- MOF-74 and Cu-MOF-74 are longer than basal M-O bonds with Cu-MOF-74 depicting elongation of 0.46 Å, which is reasonably consistent with the experimentally observed elongation of 0.53 Å. Binding enthalpies were calculated, including zero-point energy and thermal corrections with a darker colour indicating a stronger binding (Table 3, Figure 18).

Comparing the computed results with the experimental values for all M-MOF-74s, H_2, CH_4, and CO_2 exhibited appreciable results, and the values are very close to that of experiments. They showed a very small mean absolute error (MAE) of values of just 0.8 KJ/mol for H_2, 1.0 $KJmol^{-1}$ for CH_4, and 1.9 KJ/mol for CO_2. However, the MAE values for N_2 and CO are substantially higher. This might be because these molecules can be bound by electronic interactions and, thus, can cause a drastic modification of the electronic structure at the coordinatively unsaturated metal binding site. As shown in Figure 19, a noticeable trend that is unrelated to the guest molecule does emerge in the molecular binding energies in different M-MOF-74s. While proceeding across the third row of the periodic table, guest molecules generally experience rising affinity, except for dramatic drops at Cr (d^4) and Cu (d^9). The Cr-MOF-74 and Cu-MOF-74 demonstrate incredibly feeble binding for guest molecules.

As an evaluation of the vdW-DF2+U technique for estimating the enthalpies of gas adsorption, the CO_2 isosteric heat of adsorption and experimentally tested

Table 3. Computed Binding Enthalpies of the Guest Molecules in the Isostructural M-MOF-74s (in kJ/mol at 297 K). Reproduced with permission from Ref. 128 Copyright 2014 American Chemical Society.

	d^0 Mg	d^2 Ti	d^3 V	d^4 Cr	d^5 Mn	d^6 Fe	d^7 Co	d^8 Ni	d^9 Cu	d^{10} Zn
H_2	10*	17	18	6	8*	9*	9*	10*	6	8*
CH_4	19*	23	26	14	19*	19*	18*	19*	14	19*
N_2	28*	58	52	14	21	21*	21	24*	13	19
CO	35*	77	70	20	29*	30*	30*	34*	16	25*
CO_2	41*	46	51	27	34*	34*	34*	37*	27	30*
H_2S	43	57	62	30	43	42	41	45	14	39
SO_2	62	146	110	55	59	53	48	50	40	55
H_2O	62	71	77	31	51	49	48	56	24	41
NH_3	74	92	98	45	68	66	66	75	34	59
C_3H_8	24*	44	47	16	39*	39*	33*	43*	32	28*
C_2H_6	35*	38	40	32	34*	35*	35*	36*	27	33*
C_2H_2	38*	51	53	31	38*	37*	36*	37*	20	35*
C_2H_4	40*	54	56	33	41*	40*	38*	41	22	38*
C_3H_6	44*	46	70	41	55*	57*	58*	59	40	53*

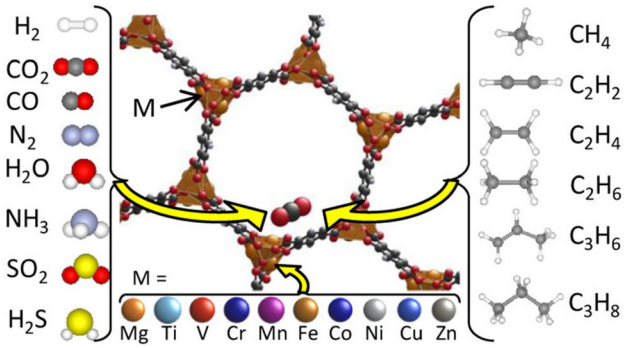

Figure 18. The representative structure of MOF taken for the investigation of M-MOF–74. Reproduced with permission from Ref. 128. Copyright 2014 American Chemical Society.

M-MOF-74s, q_{st}^{0}, was examined. With only 3-5 kJ/mol of error, their method accurately predicts the experimental adsorption temperatures and portrays the relationship between the binding enthalpies in regard to one another. On the other hand, PBE functional underestimates the binding energies as nonlocal van der Waals attraction was not considered, and PBE-D2 fails to account for this nonlocal correlation effect in different metals quantitatively. Based on their estimations of binding enthalpies, the authors could make several estimates about the prospective use of these MOFs for different gas separation and gas adsorption utilities.

This study summarizes that Mn-MOF-74 could be utilized for extracting trace flue-gas pollutants as well as poisonous gases from the air and that Cu-MOF-74 would selectively capture CO_2 against H_2O. At the same time, V-MOF-74 could be a potential material for the classic cryogenic distillation method of separating methane and nitrogen (Table 2).

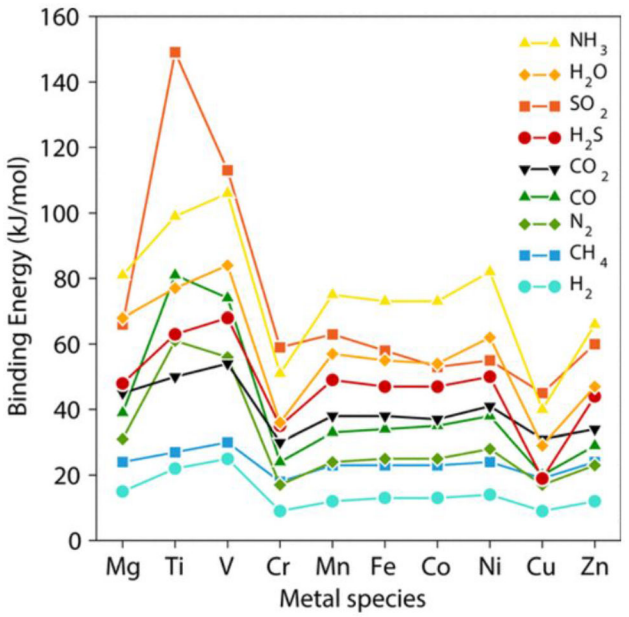

Figure 19. M-MOF-74 binding energies for a row of different small compounds on the periodic table. Reproduced with permission from Ref. 128. Copyright 2014 American Chemical Society.

7. Discussion and conclusions

Metal-Organic frameworks have emerged as a new class of materials in recent years with several potential applications, from energy harvesting to environmental protection. While more than one lakhs MOFs are reported to-date for various applications, the strategy to design a MOF for particular gas adsorption/storage is still elusive. Molecular modelling played a tremendous role in this area. DFT and pDFT studies have provided significant insights into various MOF structure/topology roles with respect to gas bindings; however, there are several pros and cons. Here we have attempted to provide an overview of various functionals employed for different gas binding and how well they compare with experiments. These methods can become a robust tool to offer design clues to enhance the storage capacity.

(a) ***Computational Methodology***: We have summarised binding energy computed employing different exchange-correlation functionals for various MOF topologies with gases such as CO_2, H_2, and CH_4. For the CO_2 gas, the correlation between experimental isosteric heat of adsorption and computed binding energies is very good for most of the MOFs studied (Figure 20). This suggests that independent of the exchange-correlation functionals employed, the DFT calculations are well-placed in reproducing the experiments. This may be attributed to the nature of CO_2 binding to various MOFs and its weak Lewis acidic character that most of the GGA functionals employed reproduce correctly.

If we move from CO_2 to H_2, the number of studies where such straight forward comparison could be made are far fewer. If we compare the experiment and theory, it is apparent that there are marked variations in some cases and a good correlation in others (See Figure 21 left). If we analyze the origin of the variation closely, it is clear that this is related to the nature of the MOF studied and the employed exchange-correlation functionals. Particularly revPBE-vdW functional is found to have the least error among reported complexes. As the binding of H_2 gas is related to the binding at the open-metal centers, the functional that

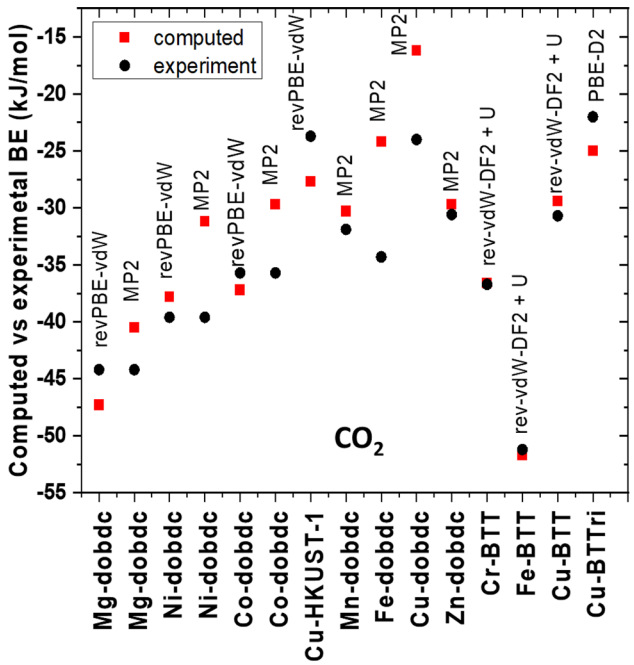

Figure 20. The computed (with different functionals) vs experimental binding energy (kJ/mol) plot for various MOFs studied here with CO_2.

can better depict the charge transfer interactions are expected to perform well.

For methane gas, the number of studies is even fewer. Still, the variations found between the experiment and theory are relatively large, and this is due to the fact that all studies have employed Perdew-Zunger LDA functional, which is known to overestimate the binding energy. Further, the methane gas binding to the metal is expected to have larger vdW contributions, often treated only in an *ad-hoc* fashion. Among the studied gas, the correlation is better for Cu^{II} MOF than other metal ions (See Figure 21 right), which suggests that semi-LDA functional employed for Cu^{II} MOFs is perhaps at an acceptable level, but it tends to get worse for other metals.

(b) ***Take Home Messages for CO_2 binding in MOFs:*** For the CO_2 gas binding on MOFs, there are several learnings from Modelling perspectives (i) while DFT calculations were able to reproduce the binding energies for this gas when charge transfer contributions are deciding factors such as those found in M_2(dobdc), one needs to adapt methodology such as MP2. In this series, it is observed that a larger charge on the metal-ion yield lower binding energies. This is correlated to the weak π-acceptor ability of CO_2, which prefers an electron-rich metal with fully filled d-shell or t_{2g} orbitals (for octahedral geometry) to facilitate greater donations. For the M-BTT family, the Fe^{II} site is found to have stronger binding for CO_2, and the binding of CO_2 at other sites of the ligands was found to be not correlated to the nature of the metal ions. As the binding of CO_2 to the ligands is purely van der Waals type interaction, ligands that have such voids and π-electron cloud could enhance the uptake capacity. Further, ligand variation from benzene-tris-tetrazolate (BTT) to benzene-tris-triazolate was found to reduce the selectivity for CO_2 over N_2, suggesting the importance of ligand design for the uptake/separation of gases.

(c) ***Take Home Messages for H_2 binding in MOFs:*** The following points are proposed to increase the uptake capacity of H_2 in MOFs, (i) decoration of MOF with light metals such as those observed in

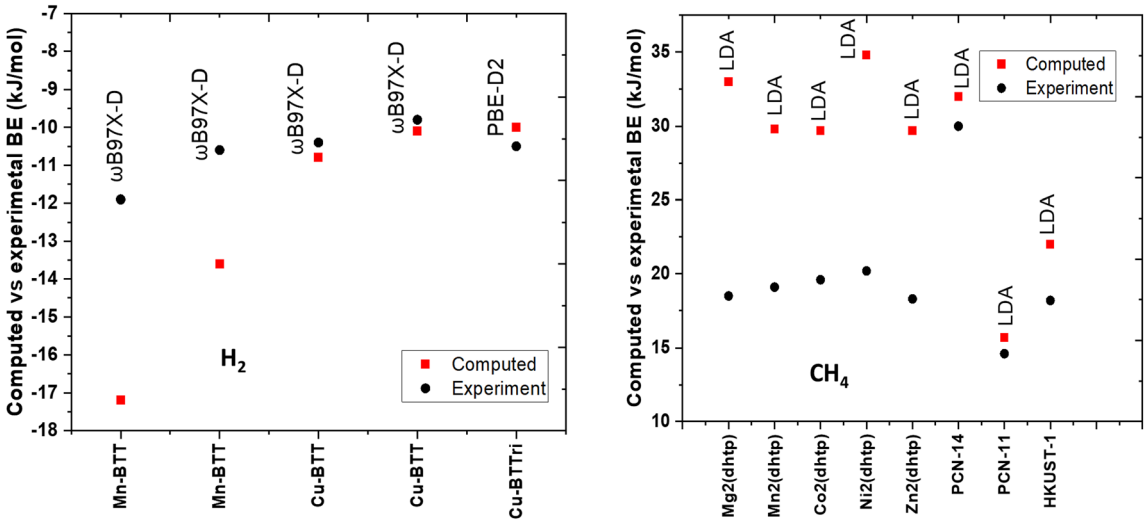

Figure 21. The computed (with different functionals) vs experimental binding energy (kJ/mol) plot for various MOFs studied here with H_2 (left) and CH_4.

calcium-decorated and boron-substituted MOF-5 (ii) employing metal ions that favours delocalization of its charge to the ligand (iii) greater volume of availability compared to halide linker also found to enhance the capacity. Among halides, F^- found to adsorb better due to great charge-transfer stabilization. (iv) Further alteration of the metal center does not found to alter the binding energy for hydrogen adsorption as the binding energy for the M-BTT series (M= Fe, Cr, Mn, Cu) ranged between 10.0 to 11.9 kJ/mol. In all cases, Van der Waal interactions are the key to regulating the hydrogen binding energy.

(d) ***Take Home Messages for O_2 binding in MOFs:*** In the case of O_2 adsorption on MOFs, (i) early transition metals were found to have substantially stronger binding for oxygen than nitrogen hence recommended for O_2/N_2 separation. This is associated with the π-acceptor ability of the metal sites, with O_2 binding to the metal being covalent in characters while N_2 binds in a van der Waals fashion. (ii) Further, ligands that are better donors that can enhance the electron donation from metal to O_2 were found to yield larger binding energy. (iii) ligand with a higher pKa leads to redox-active metal sites that are preferable for O_2 binding (iv) the acid strength of bridging anions also found to influence the O_2 binding with greater acidity leading to larger binding as stronger charge-transfer is expected (v) Our studies have concluded that the electron-transfer mechanism adopted by O_2 gives rise to Cr^{III} superoxo species ($O_2^{\cdot -}$) with a very strong antiferromagnetic coupling between the two centers, and this stabilizing exchange coupling interaction between Cr^{III} centers and oxygen leads to the spin-state-dependent binding. The adsorption isotherm calculations also demonstrate a spin-dependent binding for O_2, unlike N_2/H_2. Our study offers a new strategy for controlling gas adsorption selectivity in MOFs by applying spin-state/spin-coupling switching.

(e) ***Take Home Messages for CH_4 binding in MOFs:*** For CH_4 adsorption on MOFs the following points are crucial (i) free volume and accessible surface areas in MOFs (ii) open-metal sites found to increase the capacity where electrostatic associations among methane and open metals result in the distribution of charges and reduction of overall symmetry of CH_4 molecule. (iii) small cages/channels are also essential in methane storage, with enhanced capabilities that can be achieved by increasing the number of open metal sites, limiting the proportion of larger pores, and raising the ratio of available small channels and cages. (iv) MOFs with comparable dynamic linker freedom could provide greater CH_4 working and storage capacities.

All these summarised DFT investigations prove that there are limitless possibilities for exploring the capability of gas adsorption properties in MOFs using molecular modelling and simulation techniques. Hence, using DFT-based investigation in conjunction with experimental synthesis is an imperative tool in designing new-generation MOFs with enhanced uptake capacity.

Acknowledgements

GR and RJ would like to thank DST/SERB (SB/SJF/2019-20/12; SPR/2019/001145) for funding. GB like to thank CSIR for a fellowship.

References

1. Dincer I and Acar C 2015 A review on clean energy solutions for better sustainability *Int. J. Energy Res.* **39** 585
2. Liu S, Tang Z-R, Sun Y, Colmenares J C and Xu Y-J 2015 One-dimension-based spatially ordered architectures for solar energy conversion *Chem. Soc. Rev.* **44** 5053
3. Li W, Liu J and Zhao D 2016 Mesoporous materials for energy conversion and storage devices *Nat. Rev. Mater.* **1** 1
4. Hussain A, Arif S M and Aslam M 2017 Emerging renewable and sustainable energy technologies: State of the art *Renew. Sustain Energy. Rev.* **71** 12
5. Zhu Y P, Guo C, Zheng Y and Qiao S-Z 2017 Surface and interface engineering of noble-metal-free electrocatalysts for efficient energy conversion processes *Acc. Chem. Res.* **50** 915
6. Xie K and Wei B 2014 Materials and structures for stretchable energy storage and conversion devices *Adv. Mater.* **26** 3592
7. Hochbaum A I and Yang P 2010 Semiconductor nanowires for energy conversion *Chem. Rev.* **110** 527
8. Balzani V, Credi A and Venturi M 2008 Photochemical conversion of solar energy *Chem. Sus. Chem: Chem. Sustain. Energ. Mater.* **1** 26
9. Goldemberg J 2006 The promise of clean energy *Energy Policy* **34** 2185
10. Bonaccorso F, Colombo L, Yu G, Stoller M, Tozzini V and Ferrari AC 2015 Graphene, related two-dimensional crystals, and hybrid systems for energy conversion and storage *Science* **347**
11. Badwal S, Giddey S, Kulkarni A, Goel J and Basu S 2015 Direct ethanol fuel cells for transport and stationary applications–A comprehensive review *Appl. Energ.* **145** 80
12. Sharaf O Z and Orhan M F 2014 An overview of fuel cell technology: Fundamentals and applications *Renew. Sustain. Energ. Rev.* **32** 810

13. Li X, Hao X, Abudula A and Guan G 2016 Nanostructured catalysts for electrochemical water splitting: current state and prospects *J. Mater. Chem. A* **4** 11973
14. Roger I, Shipman M A and Symes M D 2017 Earth-abundant catalysts for electrochemical and photoelectrochemical water splitting *Nat. Rev. Chem.* **1** 1
15. Wang W, Xu X, Zhou W and Shao Z 2017 Recent progress in metal-organic frameworks for applications in electrocatalytic and photocatalytic water splitting *Adv. Sci.* **4** 1600371
16. Li X, Yu J, Low J, Fang Y, Xiao J and Chen X 2015 Engineering heterogeneous semiconductors for solar water splitting *J. Mater. Chem. A* **3** 2485
17. Rakowski Dubois M and Dubois D L 2009 Development of molecular electrocatalysts for CO_2 reduction and H_2 production/oxidation *Acc. Chem. Res.* **42** 1974
18. Langmi H W and McGrady G S 2007 Non-hydride systems of the main group elements as hydrogen storage materials *Coord. Chem. Rev.* **251** 925
19. Smith J 1980 (R.M.) Barrer. Zeolites and clay minerals as sorbents and molecular sieves. London and New York (Academic Press), 1978 viii 497 pp., 181 figs. Price £25.00 *Mineral. Mag.* **43** 829
20. Chung K-H 2010 High-pressure hydrogen storage on microporous zeolites with varying pore properties *Energy* **35** 2235
21. Li H, Wang K, Sun Y, Lollar CT, Li J and Zhou H-C 2018 Recent advances in gas storage and separation using metal–organic frameworks *Mater. Today* **21** 108
22. Ma S and Zhou H-C 2010 Gas storage in porous metal–organic frameworks for clean energy applications *Chem. Comm.* **46** 44
23. Zhou H-C, Long J R and Yaghi O M 2012 Introduction to metal–organic frameworks *Chem. Rev.* **112** 673
24. Zhang T and Lin W 2014 Metal–organic frameworks for artificial photosynthesis and photocatalysis *Chem. Soc. Rev.* **43** 5982
25. Wang C, Zhang T and Lin W 2012 Rational synthesis of noncentrosymmetric metal–organic frameworks for second-order nonlinear optics *Chem. Rev.* **112** 1084
26. Horcajada P, Gref R, Baati T, Allan P K, Maurin G and Couvreur P 2012 Metal–organic frameworks in biomedicine *Chem. Rev.* **112** 1232
27. Kreno L E, Leong K, Farha O K, Allendorf M, Van Duyne R P and Hupp J T 2012 Metal–organic framework materials as chemical sensors *Chem. Rev.* **112** 1105
28. Li J-R, Sculley J and Zhou H-C 2012 Metal–organic frameworks for separations *Chem. Rev.* **112** 869
29. Liu J, Chen L, Cui H, Zhang J, Zhang L and Su C-Y 2014 Applications of metal–organic frameworks in heterogeneous supramolecular catalysis *Chem. Soc. Rev.* **43** 6011
30. Qiu S, Xue M and Zhu G 2014 Metal–organic framework membranes: from synthesis to separation application *Chem. Soc. Rev.* **43** 6116
31. Suh M P, Park H J, Prasad T K and Lim D-W 2012 Hydrogen storage in metal–organic frameworks *Chem. Rev.* **112** 782
32. Sumida K, Rogow D L, Mason J A, McDonald T M, Bloch E D and Herm Z R 2012 Carbon dioxide capture in metal–organic frameworks *Chem. Rev.* **112** 724
33. Maurin G, Serre C, Cooper A and Férey G 2017 The new age of MOFs and of their porous-related solids *Chem. Soc. Rev.* **46** 3104
34. Furukawa H, Ko N, Go Y B, Aratani N, Choi S B and Choi E 2010 Ultrahigh porosity in metal-organic frameworks *Science* **329** 424
35. Long J R and Yaghi O M 2009 The pervasive chemistry of metal–organic frameworks *Chem. Soc. Rev*. **38** 1213
36. Kitagawa S 2014 Metal–organic frameworks (MOFs) *Chem. Soc. Rev.* **43** 5415
37. Denning S, Majid A A, Lucero J M, Crawford J M, Carreon M A and Koh C A 2020 Metal–Organic Framework HKUST-1 Promotes Methane Hydrate Formation for Improved Gas Storage Capacity *ACS Appl. Mater. Interfaces* **12** 53510
38. Mao V Y, Milner P J, Lee J H, Forse A C, Kim E J and Siegelman R L 2020 Cooperative Carbon Dioxide Adsorption in Alcoholamine-and Alkoxyalkylamine-Functionalized Metal–Organic Frameworks *Angew. Chem. Int. Ed.* **59** 19468
39. Jaffe A, Ziebel M E, Halat D M, Biggins N, Murphy R A and Chakarawet K 2020 Selective, High-Temperature O2 Adsorption in Chemically Reduced, Redox-Active Iron-Pyrazolate Metal–Organic Frameworks *J. Am. Chem. Soc.* **142** 14627
40. Kim E J, Siegelman R L, Jiang H Z, Forse A C, Lee J-H and Martell J D 2020 Cooperative carbon capture and steam regeneration with tetraamine-appended metal–organic frameworks *Science* **369** 392
41. Connolly B M, Madden D G, Wheatley A E and Fairen-Jimenez D 2020 Shaping the future of fuel: Monolithic metal–organic frameworks for high-density gas storage *J. Am. Chem. Soc.* **142** 8541
42. Morris L, Hales J J, Trudeau M L, Georgiev P, Embs J P and Eckert J 2019 A manganese hydride molecular sieve for practical hydrogen storage under ambient conditions *Energy. Environ. Sci.* **12** 1580
43. Jaramillo D E, Reed D A, Jiang H Z, Oktawiec J, Mara M W and Forse AC 2020 Selective nitrogen adsorption via backbonding in a metal–organic framework with exposed vanadium sites *Nat. Mater.* **19** 517
44. Bachman J E, Reed D A, Kapelewski M T, Chachra G, Jonnavittula D and Radaelli G 2018 Enabling alternative ethylene production through its selective adsorption in the metal–organic framework Mn2 (m-dobdc) *Energy Environ. Sci.* **11** 2423
45. Liu L, Yao Z, Ye Y, Yang Y, Lin Q and Zhang Z 2020 Integrating the Pillared-Layer Strategy and Pore-Space Partition Method to Construct Multicomponent MOFs for C_2H_2/CO_2 Separation *J. Am. Chem. Soc.* **142** 9258
46. Mizutani N, Hosono N, Le Ouay B, Kitao T, Matsuura R and Kubo T 2020 Recognition of Polymer Terminus by Metal–Organic Frameworks Enabling Chromatographic Separation of Polymers *J. Am. Chem. Soc.* **142** 3701
47. Jiang H, Yang K, Zhao X, Zhang W, Liu Y and Jiang J 2020 Highly Stable Zr (IV)-Based Metal–Organic Frameworks for Chiral Separation in Reversed-Phase Liquid Chromatography *J. Am. Chem. Soc.* **143** 390
48. Hou Q, Zhou S, Wei Y, Caro Jr and Wang H 2020 Balancing the Grain Boundary Structure and the

Framework Flexibility through Bimetallic Metal–Organic Framework (MOF) Membranes for Gas Separation *J. Am. Chem. Soc.* **142** 9582
49. Qian Q, Asinger P A, Lee M J, Han G, Mizrahi Rodriguez K and Lin S 2020 MOF-based membranes for gas separations *Chem. Rev.* **120** 8161
50. Xiao D J, Gonzalez M I, Darago L E, Vogiatzis K D, Haldoupis E and Gagliardi L 2016 Selective, tunable O_2 binding in cobalt (II)–triazolate/pyrazolate metal–organic frameworks *J. Am. Chem. Soc.* **138** 7161
51. Wang X Z, Mao X Y, Zhang Z Q, Guo R, Zhang Y Y and Zhu N J 2020 Solvothermal and Ultrasonic Preparation of Two Unique Cluster-Based Lu and Y Coordination Materials: Metal–Organic Framework-Based Ratiometric Fluorescent Biosensor for an Ornidazole and Ronidazole and Sensing Platform for a Biomarker of Amoeba Liver Abscess *Inorg. Chem.* **59** 2910
52. Hu R, Zhang X, Chi K-N, Yang T and Yang Y-H 2020 Bifunctional MOFs-based ratiometric electrochemical sensor for multiplex heavy metal ions *ACS Appl. Mater. Interfaces* **12** 30770
53. Zhu N, Gu L, Wang J, Li X, Liang G and Zhou J 2019 Novel and sensitive chemiluminescence sensors based on 2D-MOF nanosheets for one-step detection of glucose in human urine *J. Phys. Chem. C* **123** 9388
54. Andrés M A, Vijjapu M T, Surya S G, Shekhah O, Salama K N and Serre C 2020 Methanol and humidity capacitive sensors based on thin films of MOF nanoparticles *ACS Appl. Mater. Interfaces* **12** 4155
55. Zheng X, Zhao Y, Jia P, Wang Q, Liu Y and Bu T 2020 Dual-Emission Zr-MOF-Based Composite Material as a Fluorescence Turn-On Sensor for the Ultrasensitive Detection of Al^{3+} *Inorg. Chem.* **59** 18205
56. Yu K, Wei T, Li Z, Li J, Wang Z and Dai Z 2020 Construction of Molecular Sensing and Logic Systems Based on Site-Occupying Effect-Modulated MOF–DNA Interaction *J. Am. Chem. Soc.* **142** 21267
57. Yang Y, Zhang X, Kanchanakungwankul S, Lu Z, Noh H and Syed Z H 2020 Unexpected "Spontaneous" Evolution of Catalytic, MOF-Supported Single Cu (II) Cations to Catalytic, MOF-Supported Cu (0) Nanoparticles *J. Am. Chem. Soc.* **142** 21169
58. Johnson B A, Beiler A M, McCarthy B D and Ott S 2020 Transport Phenomena: Challenges and Opportunities for Molecular Catalysis in Metal–Organic Frameworks *J. Am. Chem. Soc.* **142** 11941
59. Li M, Chen J, Wu W, Fang Y and Dong S 2020 Oxidase-like MOF-818 Nanozyme with High Specificity for Catalysis of Catechol Oxidation *J. Am. Chem. Soc.* **142** 15569
60. Zhou G, Wang B and Cao R 2020 Acid Catalysis in Confined Channels of Metal–Organic Frameworks: Boosting Orthoformate Hydrolysis in Basic Solutions *J. Am. Chem. Soc.* **142** 14848
61. Peralta R A, Huxley M T, Evans J D, Fallon T, Cao H and He M 2020 Highly Active Gas Phase Organometallic Catalysis Supported Within Metal–Organic Framework Pores *J. Am. Chem. Soc.* **142** 13533
62. Tiburcio E, Greco R, Mon M, Ballesteros-Soberanas J, Ferrando-Soria Js and López-Haro M 2021 Soluble/MOF-Supported Palladium Single Atoms Catalyze the Ligand-, Additive-, and Solvent-Free Aerobic Oxidation of Benzyl Alcohols to Benzoic Acids *J. Am. Chem. Soc.* **143** 2581
63. Sanad M F, Puente Santiago A R, Tolba S A, Ahsan M A, Fernandez-Delgado O and Shawky Adly M 2021 Co–Cu bimetallic metal organic framework catalyst outperforms the Pt/C benchmark for oxygen reduction *J. Am. Chem. Soc.* **143** 4064
64. Ma W, Xie S, Zhang X-G, Sun F, Kang J and Jiang Z 2019 Promoting electrocatalytic CO_2 reduction to formate via sulfur-boosting water activation on indium surfaces *Nat. Commun.* **10** 1
65. Klontzas E, Tylianakis E and Froudakis G E 2010 Designing 3D COFs with enhanced hydrogen storage capacity *Nano. Lett.* **10** 452
66. Han S S, Furukawa H, Yaghi O M and Goddard Iii W A 2008 Covalent organic frameworks as exceptional hydrogen storage materials *J. Am. Chem. Soc.* **130** 11580
67. Dinca M, Dailly A, Liu Y, Brown C M, Neumann D A and Long J R 2006 Hydrogen storage in a microporous metal− organic framework with exposed Mn^{2+} coordination sites *J. Am. Chem. Soc.* **128** 16876
68. Bloch E D, Murray L J, Queen W L, Chavan S, Maximoff S N and Bigi J P 2011 Selective binding of O_2 over N_2 in a redox–active metal–organic framework with open iron (II) coordination sites *J. Am. Chem. Soc.* **133** 14814
69. Chen B, Yang Y, Zapata F, Lin G, Qian G and Lobkovsky E B 2007 Luminescent open metal sites within a metal–organic framework for sensing small molecules *Adv. Mater.* **19** 1693
70. Wu H, Zhou W and Yildirim T 2009 High-capacity methane storage in metal− organic frameworks M2 (dhtp): the important role of open metal sites *J. Am. Chem. Soc.* **131** 4995
71. Rana M K, Koh H S, Hwang J and Siegel D J 2012 Comparing van der Waals density functionals for CO_2 adsorption in metal organic frameworks *J. Phys. Chem. C* **116** 16957
72. Caskey S R, Wong-Foy A G and Matzger A J 2008 Dramatic tuning of carbon dioxide uptake via metal substitution in a coordination polymer with cylindrical pores *J. Am. Chem. Soc.* **130** 10870
73. Dietzel P D, Morita Y, Blom R and Fjellvåg H 2005 An in situ high-temperature single-crystal investigation of a dehydrated metal–organic framework compound and field-induced magnetization of one-dimensional metal–oxygen chains *Angew. Chem. Int. Ed.* **44** 6354
74. Chui SS Y, Lo SM F, Charmant J P, Orpen A G and Williams I D 1999 A chemically functionalizable nanoporous material $[Cu_3(TMA)_2\ (H_2O)_3]$ n *Science* **283** 1148
75. Grimme S 2006 Semiempirical GGA-type density functional constructed with a long-range dispersion correction *J. Comput. Chem.* **27** 1787
76. Kresse G and Furthmüller J 1996 Efficiency of ab-initio total energy calculations for metals and semiconductors using a plane-wave basis set *Comput. Mater. Sci.* **6** 15

77. Blöchl P E 1994 Projector augmented-wave method *Phys. Rev. B* **50** 17953
78. Grimme S 2004 Accurate description of van der Waals complexes by density functional theory including empirical corrections *J. Comput. Chem.* **25** 1463
79. Grimme S, Antony J, Ehrlich S and Krieg H 2010 A consistent and accurate ab initio parametrization of density functional dispersion correction (DFT-D) for the 94 elements H-Pu *J. Comput. Chem.* **132** 154104
80. Parr R G and Yang W 1984 Density functional approach to the frontier-electron theory of chemical reactivity *J. Am. Chem. Soc.* **106** 4049
81. Dion M, Rydberg H, Schröder E, Langreth D C and Lundqvist B I 2004 Van der Waals density functional for general geometries *Phys. Rev. Lett.* **92** 246401
82. Zhou W, Wu H and Yildirim T 2008 Enhanced H2 adsorption in isostructural metal− organic frameworks with open metal sites: strong dependence of the binding strength on metal ions *J. Am. Chem. Soc.* **130** 15268
83. Frisch M J, Head-Gordon M and Pople J A 1990 A direct MP2 gradient method *Chem. Phys. Lett.* **166** 275
84. Adler T B, Knizia G and Werner H J 2007 A simple and efficient CCSD (T)-F12 approximation *Chem. Phys.* **127** 221106
85. Yu D, Yazaydin A O, Lane J R, Dietzel P D and Snurr R Q 2013 A combined experimental and quantum chemical study of CO_2 adsorption in the metal–organic framework CPO-27 with different metals *Chem. Sci.* **4** 3544
86. Frisch M, Trucks G, Schlegel H, Scuseria G, Robb M and Cheeseman J 2009 Gaussian 09, rev *Gaussian Inc, Wallingford*
87. Becke A 1993 Density-functional thermochemistry. III The role of exact exchange *J. Chem. Phys.* **98** 564
88. Asgari M, Jawahery S, Bloch E D, Hudson M R, Flacau R and Vlaisavljevich B 2018 An experimental and computational study of CO_2 adsorption in the sodalite-type M-BTT (M= Cr, Mn, Fe, Cu) metal–organic frameworks featuring open metal sites *Chem. Sci.* **9** 457
89. Kresse G and Hafner J 1993 Ab initio molecular dynamics for liquid metals *Phys. Rev. B* **47** 558
90. Giannozzi P, Baroni S, Bonini N, Calandra M, Car R and Cavazzoni C 2009 QUANTUM ESPRESSO: a modular and open-source software project for quantum simulations of materials *J. Phys. Condens.* **21** 395502
91. Ernzerhof M and Scuseria G E 1999 Assessment of the Perdew–Burke–Ernzerhof exchange-correlation functional *J. Chem. Phys.* **110** 5029
92. Goings J J, Ohlsen S M, Blaisdell K M and Schofield D P 2014 Sorption of H2 to Open Metal Sites in a Metal–Organic Framework: A Symmetry-Adapted Perturbation Theory Analysis *J. Phys. Chem. A* **118** 7411
93. Kuc A, Heine T, Seifert G and Duarte H A 2008 H2 Adsorption in Metal-Organic Frameworks: Dispersion or Electrostatic Interactions? *Chem. Eur. J.* **14** 6597
94. Kumar R M and Subramanian V 2011 Interaction of H2 with fragments of MOF-5 and its implications for the design and development of new MOFs: A computational study *Int. J. Hydrog. Energy* **36** 10737
95. Agusta M K, Saputro A G, Tanuwijaya V V, Hidayat N N and Dipojono H K 2017 Hydrogen adsorption on Fe-based metal organic frameworks: DFT study *Procedia. Eng.* **170** 136
96. Kancharlapalli S, Gopalan A, Haranczyk M and Snurr R Q 2021 Fast and accurate machine learning strategy for calculating partial atomic charges in metal–organic frameworks *J. Chem. Theory. Comput.* **17** 3052
97. Lin X, Telepeni I, Blake A J, Dailly A, Brown C M and Simmons J M 2009 High capacity hydrogen adsorption in Cu (II) tetracarboxylate framework materials: the role of pore size, ligand functionalization, and exposed metal sites *J. Am. Chem. Soc.* **131** 2159
98. Wang Z and Cohen S M 2009 Postsynthetic modification of metal–organic frameworks *Chem. Soc. Rev.* **38** 1315
99. Bhatia S K and Myers A L 2006 Optimum conditions for adsorptive storage *Langmuir* **22** 1688
100. Hübner O, Glöss A, Fichtner M and Klopper W 2004 On the interaction of dihydrogen with aromatic systems *J. Phys. Chem. A* **108** 3019
101. Arean C O, Bonelli B, Delgado M R and Garrone E 2009 Hydrogen storage via physisorption: the combined role of adsorption enthalpy and entropy *Turk. J. Chem.* **33** 599
102. Areán C O, Chavan S, Cabello C P, Garrone E and Palomino G T 2010 Thermodynamics of hydrogen adsorption on metal-organic frameworks *Chem. Phys. Chem.* **11** 3237
103. Sumida K, Stück D, Mino L, Chai J-D, Bloch E D and Zavorotynska 2013 Impact of metal and anion substitutions on the hydrogen storage properties of M-BTT metal–organic frameworks *J. Am. Chem. Soc.* **135** 1083
104. Zou X, Cha M-H, Kim S, Nguyen M C, Zhou G and Duan W 2010 Hydrogen storage in Ca-decorated, B-substituted metal organic framework *Int. J. Hydrog. Energy.* **35** 198
105. Dixit M, Adit Maark T, Ghatak K, Ahuja R and Pal S 2012 Scandium-decorated MOF-5 as potential candidates for room-temperature hydrogen storage: a solution for the clustering problem in MOFs *J. Phys. Chem. C* **116** 17336
106. Li H, Eddaoudi M, O'Keeffe M and Yaghi O M 1999 Design and synthesis of an exceptionally stable and highly porous metal-organic framework *Nature* **402** 276
107. Schoedel A and Yaghi O M 2016 Porosity in metal–organic compounds *Macrocyc. Supramol. Chem.* **20** 201
108. Ghosh D, Kosenkov D, Vanovschi V, Flick J, Kaliman I and Shao Y 2013 Effective fragment potential method in Q-CHEM: A guide for users and developers *J. Comput. Chem.* **34** 1060
109. Parr R G 1980 Density Functional Theory of Atoms and Molecules. In: *Horizons of Quantum Chemistry. Académie Internationale Des Sciences Moléculaires Quantiques/International Academy of Quantum Molecular Science* Vol 3. K Fukui and B Pullman (Eds.) (Dordrecht: Springer)
110. Asgari M, Semino R, Schouwink P, Kochetygov I, Trukhina O and Tarver J D 2019 An In-Situ Neutron

Diffraction and DFT Study of Hydrogen Adsorption in a Sodalite-Type Metal–Organic Framework, Cu-BTTri *Eur. J. Inorg. Chem.* **2019** 1147
111. Parkes M V, Sava Gallis D F, Greathouse J A and Nenoff T M 2015 Effect of metal in $M_3(btc)_2$ and $M_2(dobdc)$ MOFs for O_2/N_2 separations: A combined density functional theory and experimental study *J. Phys. Chem. C* **119** 6556
112. Xie L, Liu S, Gao C, Cao R, Cao J and Sun C 2007 Mixed-valence Iron (II, III) trimesates with open frameworks modulated by solvents *Inorg. Chem.* **46** 7782
113. Bloch E D, Queen W L, Krishna R, Zadrozny J M, Brown C M and Long J R 2012 Hydrocarbon separations in a metal-organic framework with open iron (II) coordination sites *Science* **335** 1606
114. Dietzel P D, Panella B, Hirscher M, Blom R and Fjellvåg H 2006 Hydrogen adsorption in a nickel based coordination polymer with open metal sites in the cylindrical cavities of the desolvated framework *Chem. Comm.* **9** 959
115. Dietzel P D, Johnsen R E, Blom R and Fjellvåg H 2008 Structural changes and coordinatively unsaturated metal atoms on dehydration of honeycomb analogous microporous metal–organic frameworks *Chem. Eur. J.* **14** 2389
116. Dietzel P D, Blom R and Fjellvåg H 2008 Base-induced formation of two magnesium metal-organic framework compounds with a bifunctional tetratopic ligand *Eur. J. Inorg. Chem.* **23** 3624
117. Aquilante F, Autschbach J, Carlson R K, Chibotaru L F, Delcey M G, De Vico L, Fdez Galván I, Ferré N, Frutos L M, Gagliardi L, Garavelli M, Giussani A, Hoyer C E, Li Manni G, Lischka H, Ma D, Malmqvist P Å, Müller T, Nenov A, Olivucci M, Pedersen T B, Peng D, Plasser F, Pritchard B, Reiher M, Rivalta I, Schapiro I, Segarra-Martí J, Stenrup M, Truhlar D G, Ungur L, Valentini A, Vancoillie S, Veryazov V, Vysotskiy V P, Weingart O, Zapata F and Lindh R 2016 Molcas 8: New capabilities for multiconfigurational quantum chemical calculations across the periodic table *J. Comput. Chem.* **37** 506
118. Rosen A S, Mian M R, Islamoglu T, Chen H, Farha O K and Notestein J M 2020 Tuning the redox activity of metal–organic frameworks for enhanced, selective O_2 binding: Design rules and ambient temperature O_2 chemisorption in a cobalt–triazolate framework *J. Am. Chem. Soc.* **142** 4317
119. Jose R, Kancharlapalli S, Ghanty T K, Pal S and Rajaraman G 2022 The decisive role of spin states and spin coupling in dictating selective O_2 adsorption in chromium (II) metal–organic frameworks *Chem. Eur. J.* **28** e202104526
120. Dubbeldam D, Calero S, Ellis D E and Snurr R Q 2016 RASPA: molecular simulation software for adsorption and diffusion in flexible nanoporous materials *Mol. Simul.* **42** 81
121. Rappé A K, Casewit C J, Colwell K, Goddard III W A and Skiff W M 1992 UFF, a full periodic table force field for molecular mechanics and molecular dynamics simulations *J. Am. Chem. Soc.* **114** 10024
122. Potoff J J and Siepmann J I 2001 Vapor–liquid equilibria of mixtures containing alkanes, carbon dioxide, and nitrogen *AIChE J.* **47** 1676
123. Wang S 2007 Comparative molecular simulation study of methane adsorption in metal− organic frameworks *Energy Fuels* **21** 953
124. Kaminski G A, Friesner R A, Tirado-Rives J and Jorgensen W L 2001 Evaluation and reparametrization of the OPLS-AA force field for proteins via comparison with accurate quantum chemical calculations on peptides *J. Phys. Chem. B* **105** 6474
125. Wu H, Simmons J M, Liu Y, Brown C M, Wang X S and Ma S 2010 Metal–organic frameworks with exceptionally high methane uptake: where and how is methane stored? *Chem. Eur. J.* **16** 5205
126. Li L, Yang J, Li J, Chen Y and Li J 2014 Separation of CO_2/CH_4 and CH_4/N_2 mixtures by M/DOBDC: A detailed dynamic comparison with MIL-100 (Cr) and activated carbon *Micropor. Mesopor. Mater.* **198** 236
127. Li B, Wen H M, Zhou W and Chen B 2014 Porous metal–organic frameworks for gas storage and separation: what, how, and why? *J. Phys. Chem. Lett.* **5** 3468
128. Lee K, Howe J D, Lin L C, Smit B and Neaton J B 2015 Small-molecule adsorption in open-site metal–organic frameworks: a systematic density functional theory study for rational design *Chem. Mater.* **27** 668
129. Rana M K, Koh H S, Hwang J and Siegel D J 2012 Comparing van der Waals density functionals for CO_2 adsorption in metal-organic frameworks *J. Phys. Chem. C* **116** 16957
130. Britt D, Tranchemontagne D and Yaghi O M 2008 Metal-organic frameworks with high capacity and selectivity for harmful gases *Proc. Natl. Acad. Sci.* **105** 11623
131. Bao Z, Yu L, Ren Q, Lu X and Deng S 2011 Adsorption of CO_2 and CH_4 on a magnesium-based metal organic framework *J. Colloid. Interface. Sci.* **353** 549
132. Wang Q M, Shen D, Bülow M, Lau M L, Deng S and Fitch F R 2002 Metallo-organic molecular sieve for gas separation and purification *Micropor. Mesopor. Mater.* **55** 217
133. Liang Z, Marshall M and Chaffee A L 2009 CO_2 adsorption-based separation by metal organic framework (Cu-BTC) versus zeolite (13X) *Energy Fuels* **23** 2785
134. Farrusseng D, Daniel C, Gaudillere C, Ravon U, Schuurman Y and Mirodatos C 2009 Heats of adsorption for seven gases in three metal− organic frameworks: systematic comparison of experiment and simulation *Langmuir* **25** 7383
135. Sanz R, Martínez F, Orcajo G, Wojtas L and Briones D 2013 Synthesis of a honeycomb-like Cu-based metal–organic framework and its carbon dioxide adsorption behaviour *Dalton. Trans.* **42** 2392
136. Asgari M, Jawahery S, Bloch E D, Hudson M R, Flacau R and Vlaisavljevich B 2018 An experimental and computational study of CO_2 adsorption in the sodalite-type M-BTT (M= Cr, Mn, Fe, Cu) metal–organic frameworks featuring open metal sites *Chem. Sci.* **9** 4579

137. Asgari M, Semino R, Schouwink P A, Kochetygov I, Tarver J and Trukhina O 2020 Understanding how ligand functionalization influences CO_2 and N_2 adsorption in a sodalite metal–organic framework *Chem. Mater.* **32** 1526
138. Bloch E D, Queen W L, Hudson M R, Mason J A, Xiao D J and Murray L J 2016 Hydrogen storage and selective, reversible O_2 adsorption in a metal–organic framework with open chromium (II) sites *Angew. Chem.* **128** 8747
139. Zhou W, Wu H, Hartman M R and Yildirim T 2007 Hydrogen and methane adsorption in metal− organic frameworks: a high-pressure volumetric study *J. Phys. Chem. C* **111** 16131
140. Senkovska I and Kaskel S 2008 High pressure methane adsorption in the metal-organic frameworks $Cu_3(btc)_2$, $Zn_2(bdc)_2dabco$, and $Cr_3F(H_2O)_2O(bdc)_3$ *Micropor. Mesopor. Mater.* **112** 108